NASA TECHNICAL MEMORANDUM NASA TM-75146

ACOUSTIC CONDITIONS IN THE VICINITY OF AN ORIFICE THAT DEPENDS ON GRAZING FLOW BOUNDARY LAYERS

AN EXPERIMENTAL INVESTIGATION

Jurgen Kompenhans

Translation of "Das Akustische Verhalten Überströmter Öffnungen in Abhängigkeit von der Wandgrenzschicht, eine Experimentelle Untersuchung" Doctoral Dissertation, Goettingen University, Goettingen, West Germany, pp. 1-58, 1976.

NATIONAL AERONAUTICS AND SPACE ADMINISTRATION
WASHINGTON, D. C. 20546 NOVEMBER 1977

STANDARD TITLE PAGE

1. Report No. NASA TM-75146	2. Government Accession No.	3. Recipient's Catalog No.
4. Title and Subtitle Acoustic Conditions in the Vicinity of an Orifice that Depends on Grazing Flow Boundary Layers - an Experimental Investigation.		5. Report Date November, 1977 6. Performing Organization Code
7. Author(s) Jurgen Kompenhans		8. Performing Organization Report No. 10. Work Unit No.
9. Performing Organization Name and Address SCITRAN Box 5456 Santa Barbara, CA 93108		11. Contract or Grant No. NASw-2791 13. Type of Report and Period Covered Translation
12. Sponsoring Agency Name and Address National Aeronautics and Space Administration Washington, D.C. 20546		14. Sponsoring Agency Code

15. Supplementary Notes

Translation of "Das Akustische Verhalten Uberstromter Öffnungen in Abhängigkeit Von Der Wandgrenzschicht Eine Experimentelle Untersuchung" Doctoral Dissertation, Goettingen University, Goettingen, West Germany, pages 1-58, 1976.

16. Abstract

The reflection factor at the end of a tube which ends at a plate over which a flow is forming was determined as a function of the Strouhal number, formed from the flow velocity, the aperture radius, and the acoustic frequency.

We investigated two or nine adjacent openings, in order to investigate the questions of interactions between several openings.

17. Key Words (Selected by Author(s))	18. Distribution Statement
	Unclassified - Unlimited

19. Security Classif. (of this report)	20. Security Classif. (of this page)	21. No. of Pages	22. Price
Unclassified	Unclassified	62	

ACOUSTIC CONDITIONS IN THE VICINITY OF AN ORIFICE THAT DEPENDS ON GRAZING FLOW BOUNDARY LAYERS. AN EXPERIMENTAL INVESTIGATION

Jurgen Kompenhans

SUMMARY /I*

The reflection factor at the end of a tube which ends at a plate over which a flow is flowing was determined as a function of the Strouhal number, formed from the flow velocity, the aperture radius, and the acoustic frequency.

It is possible to calculate the flow end correction from this reflection factor. The loss contribution of the opening impedance increases as a function of the flow velocity, and it decreases as a function of mass fraction. The ratio of the displacement thickness of the flow above the opening and the opening radius is found to be an important parameter. Especially the real part of the opening impedance can be represented as a function of this ratio for small Strouhal numbers. As the boundary layer becomes thicker, the loss coefficient of the opening impedance decreases. Measurements of the direct flow resistance of the opening confirm this relationship. The decrease of the mass fraction of the impedance is determined for the most part by the Strouhal number and the boundary layer thickness.

When the opening length becomes comparable to the opening radius, then there are additional changes in the opening impedance, which probably can be attributed to the influence of flow fluctuations on the inner mouth of the opening.

Various modifications of the opening inner edge, such as rounding off, also change the opening impedance.

We investigated two or nine adjacent openings in order to investigate the questions of interactions between several openings.

---

*Numbers in margin indicate pagination in foreign text.

TABLE OF CONTENTS

/II

/III

LIST OF SYMBOLS /IV

a	opening radius
b	distance between opening and center of measurement tube.
c	speed of sound ($c = 343.8$ m/s)
f	frequency
i	imaginary unit
k	wave number ($k = \omega/c$)
l	opening length
i_{Ek}	length of end correction of the opening
l_{Ek_i}	length of inner end correction of opening.
p	acoustic pressure
r_{Ek}	reflection factor in the plane of the upper edge of opening
u	flow velocity component in the direction of the channel flow
v_G	flow velocity through the opening
y	wall separation
A_{akust}	inclination of line for the real part of the opening impedance for the quasi-stationary range $R/X_o = A_{akust} \cdot S^{-1} + B$
A_{stat}	normalized uniform flow resistance (section 5)
H	shape parameter $(H = \delta^*/\vartheta)$
P	pressure
R	real part of impedance of end correction
R_G	additional uniform flow resistance of opening caused by overflow
R_R	radius of measurement tube
R_S	total uniform flow resistance of opening ($R_S = R_o + R_G$)
R_o	uniform flow resistance of opening for air at rest
S	Strouhal number ($S = a\omega/U$)
S^{-1}	reciprocal Strouhal number ($S^{-1} = U/a\omega$)
U	flow velocity in center of channel
W_{Ek}	end correction normalized with X_o
X	imaginary part of end correction impedance
X_o	imaginary part of impedance of end correction for air at rest ($X_o \approx 0.85\, a\rho\omega$)
Z_{Ek}	impedance of end correction ($Z_{Ek} = R = iX$)
Z_{rohr}	impedance of infinitely long tube

/V

γ	Gradient of normalized boundary layer profile in vicinity of wall.(section 4).
δ^*	Displacement thickness
ϑ	Momentum loss thickness
ξ	Opening radius/effective opening radius ($\xi = \sqrt{\sigma}$)
ρ	Density of the medium (for air $\rho = 1.205$ kg/m^3)
σ	Cross section area of openings/cross section area of measurement tube.
ϕ	Phase angle
Ψ	Fok's function (section 3.3.3)
ω	Circular frequency ($\omega = 2\pi f$)
akust	acoustical
Rohr	tube
stat	stationary.

1. Introduction

/1

In order to reduce sound propagation in channels, usually the channel walls are covered with a sound-absorbing material. When the acoustic impedance of the wall covering is appropriately selected, optimum damping can be obtained. The same method is used for flows in channels; for example, in modern aircraft design, designers wish to reduce the pressure noise up to the outlet from the engine as much as possible. The absorbers usually are thin perforated sheets, because of weight and cost considerations, which are attached at a certain distance ahead of the channel wall. The space is divided like a honeycomb, in order to prevent sound propagation and flow. The acoustic impedance of the wall, in this case, consists of the impedance of the cavity and the openings.

It is found that the acoustic impedance of the openings depend greatly on the tangential flow.* Up to the present, this effect has been studied many times, especially in connection with application for engine design.

For a better understanding, it is appropriate to first consider the acoustic behavior of an opening, in quiet air. It is important that the air particles oscillate outside of the mouth of the opening as well, which provide an additional contribution to the acoustic impedance of the opening, and therefore bring about a greater effective length of the opening. (see for example, [1-7]). This additional length is called the end correction. Experimental investigations have shown that the end correction is the same for the friction part and the mass /2
part of the impedance [4, 6]. In the case of large acoustic pressures, or speeds of sound through the opening, which often occurs in practice, the opening becomes nonlinear. In other words, there is no linear relationship between the acoustic pressure and the speed of sound. [4, 7, 10]. The same is true for perforated plates [11].

If a uniform flow is superimposed on the original flow, then the conditions become more complicated. When the flow passes through the opening, then the resistance of the opening increases with flow velocity and the mass fraction decreases [10, 12].

In the case where there is tangential flow over the opening, there is also an increase in the real part and a decrease in the imaginary part of the impedance of a single opening [14, 15]. Similar behavior

*Translator's note: Flow parallel to the opening.

can also be found for various wall linings [12, 13, 16].

The measurement of the acoustic impedance of openings when there is flow superposition is very difficult, because the acoustic parameters such as the acoustic pressure and the speed of sound must be measured very accurately, both in amplitude and phase. A number of measurement techniques have been tested for measuring the impedance, and the most important ones are given in [16].

A few of the authors mentioned above first measured the uniform flow resistance of the opening, that is, at the frequency $\omega = 0$, in order to obtain an idea about the acoustic behavior of the opening, when there is flow passing through or over it. Exact investigations of the behavior of flow of openings with tangential flow showed that, depending on the direction of flow, the uniform flow resistance of the opening can change [17, 18]. The reason for this is that on one side of the opening the channel flow is situated with its wall boundary layer, and at the other side there is almost still air. The various experimental results are not yet sufficient to describe the interaction between the sound and the flow, and to correctly describe the opening theoretically. /3
Therefore various experiments were made to visualize the flow processes in the opening, for example, already 25 years ago for the non-linear case [4, 8]. More recently model experiments have been made where the flow over the opening and in the opening throat was measured in the water tunnel using colored ink [19, 20]. In the case of [19], we can see how much the flow changes in the opening between the inlet and the outlet flow process. First, a region is formed at the trailing edge of the opening where fluid flows into the opening. The colored stream line, which starts at the leading edge of the opening, penetrates into the opening throat and can roll up to form vortices. During the outflow process, the shear layer is then lifted off at the trailing edge, just like a cover.

In other model experiments [20], the ratio of the speed through the opening and the tangential flow velocity was smaller. On the pictures one can clearly see a wave-like motion of the shear layer which increases with path length, located above the opening. It is the acoustic pressure gradient which brings about this deflection of the shear layer at the leading edge. At the trailing edge of the opening, fluid flows into or out of the opening, depending on the deflection of the shear

layer.

The statements made above about the motions of the shear layer above the opening essentially agree with the assumption which Ronneburger [14] used for his model to develop the theory of acoustic impedance of openings with tangential flow. Other authors such as Mungur [21], used the idea that a vortex rotates in the opening, and thus influences the impedance. Rice [22] assumes that the opening /4
is given an additional turbulent velocity because of the tangential flow, which then leads to the same effects as for transverse flow.

One other theoretical idea is to expand the relationship of Crandall [23] or Tijdeman [24] for the non-linear case, for the sound propagation in the tube for air at rest (for example, Hersh and Rogers [25]). As the next step, we must then introduce the tangential flow. However, in [26], then the flow conditions above the opening are greatly simplified.

For the case of uniform flow through the opening, Hersh and Rogers [8] used a model with a coverlike motion of the shear layer above the opening, for comparison with their experiments.

In addition, there are papers such as the one of Moehring [27], where the separation of a thin vortex layer from a plate edge is steady. Comparisons with measurements are difficult because the parameters involved cannot be measured directly. However, if one wishes to not only use perforated plates as absorbers in channels with flow, as mentioned at the beginning, but if we are interested in a better understanding of the physical processes, in the opening, then one must first attempt to separate the various effects mentioned above, even though they occur together in practice.

The investigation presented here discusses only the case of the opening with tangential flow. The effects caused by the non-linearity or the /5
transverse flow through the opening are not important for these measurements. In order to further simplify our problem, we will only consider a single opening at first. These results are then compared later on with those for two or nine openings. By making the most accurate possible measurement of the acoustic impedance of openings, for various transverse flows, (laminar, turbulent, thick, and thin boundary layers) and the simultaneous determination of all the other acoustic and physical parameters, we will attempt to establish relationships between all

parameters.

2. Problem Formulation and Measurement Principle

The acoustic impedance of an opening is found as a ratio of acoustic pressure between both sides of the opening and the acoustic speed thru the opening. The pressure and the velocity are to be measured, in terms of phase and magnitude.

The impedance of the opening essentially consists of a mass part which can be attributed to the air particles, which oscillate in the throat of the opening and in the vicinity of the opening. The friction losses in the opening are small compared to these. The particles which participate on one side, outside of the opening throat, bring about an increase in the effective length of $l_{Ek} = 0.85\ a$ (a = radius of opening) compared with the geometric length of the opening. If the opening has a tangential flow, then the end correction of the channel side is changed, for example, the real part of the impedance (that is the losses) increases with flow velocity and the imaginary part decreases. From visual observations in the water tunnel we can see that the interaction mechanisms between the sound and the flow over the opening are very complicated. Up to now there is no theory /6 which completely describes these processes, so that no quantitative comparison with measurements is possible. Which of the flow parameters such as the center velocity, boundary layer thickness, boundary layer profile shape, or which combination of them determine the opening impedance cannot be stated at the beginning. Consequently, it is necessary to also determine the flow parameters as much as possible during acoustic measurements. Since only the flow in the vicinity of the wall has an influence on the change in the end correction, we measured the shear profile over the opening for each impedance measurement. We assumed that this contains all of the parameters important for the impedance change. In experiments it is not possible to easily vary the properties of the flow near the wall, but it is easier to change the acoustic parameters (frequency or acoustic pressure). For example, the shape and thickness of the boundary layer profile in the case of a closed channel used here can be found from the design of the channel and the installations in the channel. By changing the length of a plate, located in the channel center with flow, it is possible to adjust the

boundary layer thickness approximately using the path length of the boundary layer on the plate.

The changes which occur in the end correction when the opening has tangential flow require one to exactly measure the magnitude and phase of the acoustic pressure and the speed of sound. Depending on the experimental conditions, there are strong pressure and velocity fluctuations which are superimposed on both signals. Of course the disturbances in these variables being measured should be small as possible. Therefore, we will attempt to dispense with the measurement of the speed of sound, because the ratio of the speed amplitude and the turbulent velocity fluctuations are substantially less favorable for the speed than is the ratio of the acoustic pressure and turbulent pressure fluctuations in the case of the pressure. /7

We will dispense with measuring the speed of sound, but it is necessary to determine the sound pressure gradient or the sound pressure at various points of an acoustic line having a known impedance. This can be done by attaching microphones at various points of the tube. From the complex sound pressure amplitude measured with sound, (for example, with phase and magnitude), the reflection factor at the end of the tube can be calculated. The tube which emerges into the plate with the flow is the opening proper. Therefore, from the reflection factor in the plane of the opening edge we can immediately calculate the acoustic impedance of the correction of the opening. Using this configuration, in contrast to the measurement technique described in [14, 15] it becomes possible to measure the acoustic pressure even for large disturbances as occur in turbulent flows.

In order to exactly measure the magnitude and phase of the acoustic pressure, it is necessary to calibrate the microphones. For this purpose, the tube is irradiated with sound from both sides in sequence. The ratio of the acoustic pressures at each location is measured, and this leads to a cancelling of the complex calibration factors. In the remainder of the evaluation, only the acoustic pressure ratios are involved.

3. Measurement of Acoustic Impedance of an Opening with Tangential Flow

3.1 Measurement Setup

3.1.1 Wind Tunnel

The air from the laboratory was sucked into the test section (cross-section area, 25:1) through a settling path with flow stabilizers and hole seives, and also through a contraction path (contraction ratio 10 x 10 cm^2), (see Figure 1). There is an acoustic damper between the /8
test section and the suction blower. Then the air is blown off to the outside. In this way, heating of the air in the blower does not lead to changes in the air temperature within the test section. However, we must accept the fact that there is under pressure compared with the surroundings in the tunnel; therefore, the ceiling of the installed components (measurement tube) in the tunnel is very important.

The top side of the tunnel is covered with a plate, and there is a support for hot wire measurements (boundary layer profile) which can be displaced in the longitudinal direction. Upstream, ahead of the impedance measurement tube, it is possible to install plates of various lengths (from 5.5 cm to 65.5 cm) in the center of the tunnel. There is a wake plate 30 cm long downstream from the opening. A rotatable wing is the final part. By changing the wing position, it is possible to equalize the difference in the flow resistances of the two partial tunnels above and below the plate, and to avoid oblique flow along the plate leading edge. When there is optimum adjustment, the degree of turbulence of the channel flow reaches 0.5%. However, there is also the possibility to force a strongly turbulent flow above the opening using the wing.

3.1.2 Acoustic Part of the Measurement Instrumentation

The apparatus for measuring the opening impedance consists of a tube 110 mm long (measurement tube [A], diameter 4 mm) which opens into the plate located in the center of the tunnel, and thus forms the opening. There were thin taps (diameter 0.5 mm) separated by 10 mm in the tube. The taps are distributed statistically around the tube /9
circumference, so that higher modes of the acoustic field would average out during the measurement. (This aspect is especially important for measurement tube B because of the cross-section jump). Directly behind each tube there is a condenser microphone, type [Sell] (diameter 11 mm).

The results of [28] were considered when the microphones were built. The microphones were sealed with respect to the outside in order to prevent a flow through the tube. There is a flow resistance element at the lower end of the tube. The tube is closed off by means of a 35-watt pressure chamber loudspeaker. The tube was subjected to acoustic irradiation from the side of the tunnel by using a loudspeaker attached to the tunnel wall. However, the sound pressure amplitudes for this in the tunnel were so large, that a plate which is rigidly connected to the impedance measurement tube was excited to body oscillations. In order to exclude this source of error, a loudspeaker with a short attachment tube was installed above the measurement tube.(Figure 1). The loudspeaker was then placed directly on the opening during calibrations. The static pressure between the tunnel and the measurement tube was equalized by means of a small hole in the attachment tube.

A slightly modified configuration was used for the second part of the investigations (measurement tube B, Figure 2). Now the measurement tube has a diameter of 20 mm. Exchangeable discs can be inserted with the appropriate opening along the top side. Therefore, it is possible to investigate openings with various thicknesses, edge roundings, or even several openings in a relatively simple manner. Table 1 gives a summary about the openings investigated.

3.1.3 Electronic Part of the Measurement Installation /10

After the first measurements, it was realized that the acoustic sound variation in the tube could not be scanned accurately enough for the later evaluation by only using two or four microphones, and therefore the electronics developed in [28] for the exact measurement of acoustic damping in tubes was employed. The main problem in both cases was the fact that it was difficult to measure the magnitude and phase of an acoustic pressure signal which was highly contaminated by flow noise. This is best done using phase-sensitive rectifiers, which filter out the zero-degree and 90-degree component of the signals. In order to allow a faster recording of all 10 acoustic pressures, a special phase-sensitive rectifier was required for each microphone. In order to avoid phase errors between the reference voltages, for phase-sensitive rectification, all the electrical signals were drawn off from a common frequency generator which had digital adjustment (Figure

3). The frequency generator is operated at 24 times the measurement frequency, and controls a 12-bit shift register in a digital sine generator. The output of it is inverted and coupled back to the input. For example, if the shift register is completely empty at the beginning, then a rectangular pulse with a length corresponding to 24 timing intervals runs in it at the measurement frequency. By using a suitable resistance matrix, controlled by the outputs of the shift register, it is possible to generate from this a step sinusoidal signal.

The advantage of ths method is found if one wishes to produce a signal which is phase-displaced with respect to the first signal. In this case, an additional rectangular signal runs in the second shift register, which can be displaced by one or several timing intervals with respect to the first. In this way one obtains a sine signal which is frequency-independent and is displaced by exactly a multiple of 15° /11 with respect to the first one. (12 timing intervals correspond to 180°).

The higher harmonics contained in the step sine signals were filtered out using a tertiary filter. After this, the zero-degree signal was applied alternately to the two loudspeakers through a force amplifier. The reference signals of zero degrees and 90 degrees for the phase sensitive rectifier were also derived from the form of two-phase-displaced rectangular signals from the digital sine generator. After phase-sensitive rectification, the direct voltages corresponding to the zero-degree and 90-degree component of the acoustic pressure signals were supplied within 0.5 seconds to a A/D converter through a multiplexer. Then they were stored on magnetic tape.

The big advantage of this method is the fact that all signals can be derived from a common controlled signal. The reference voltages, as well as the phase-displaced signals for the later-to-be-described calibration are therefore produced in digital form and with great accuracy. In particular, the phase relationships of the reference signals do not change with frequency.

3.2. Measurement Procedure

Even though the phase-sensitive rectifiers used are not very complex, they provide a real and imaginary part of the amplitude input signal quite accurately. In order to measure the phase relationships between the pressure signals even more accurately, the phase-rectifiers are also calibrated as done in [28]. At the beginning of each measurement series,

a signal with constant amplitude, which is displaced in steps of 15°, with respect to the reference signal each time, is given to the phase-sensitive rectifier. From the output voltages, a correction vector is /12
then calculated for each channel. It is found that this correction vector changes linearly with frequency, in other words, the calibration only has to be performed at the lowest and the highest frequency of each measurement series. Interpolation is performed in between.

The measurement itself is done by first irradiating the tube by the loudspeaker 1 (Figure 3). For each of the zero-degree and 90-degree components of the ten-channels of the phase-sensitive rectifiers, 32 scanned values are stored on magnetic tape. Depending on the magnitude of the turbulent pressure fluctuations, this measurement is repeated in short intervals up to 25 times in order to obtain good time averaging. Of course, the fast recording of a large number of data points is advantageous, which becomes possible by storing on tape. After this the loudspeaker 2 with the attachment tube is placed on the opening, and the measurement is repeated.

One disadvantage of this method is that measuring and evaluation are completely separate. During the measurement, one can note and establish whether the measurement results are meaningful. Another disadvantage is the dependence on an EDP installation required for the evaluation.

3.3 Evaluation

3.3.1 Sound Pressure Variation in the Measurement Tube

The acoustic pressure measured in the individual microphones is first averaged, and then is corrected for errors of the phase-sensitive rectifiers. The calibration factors of the microphones are eliminated by dividing the ten complex acoustic pressures for irradiation of the tube from the inside and the outside by each other. In this way we /13
have an acoustic pressure ratio at each microphone location.

The acoustic wave which comes in from the outside is reflected at the flow resistance element at the low end of the tube. The acoustic wave from the loudspeaker 1 is reflected at the air particles which are oscillating outside of the tube (end correction). More detail can be found in the appendix. By matching with the measured acoustic pressure ratios, it is possible to very exactly determine the (unknown)

reflection factors at both ends of the measurement tube.

In order to calculate the impedence of the end correction, during the subsequent evaluation we use the reflection factor which has been determined in the plane of the opening upper edge. Consequently, in the case of tangential flow, we act as though the sound propagation in the tube is undisturbed up to the opening edge. All of the changes caused by the flow are then contained in the impedance of the end correction. This will be discussed in section 6.3.1.

The equalization calculation as was used in [28] for determining the acoustic damping in tubes was taken over for our conditions. For the theoretical sound propagation in the tube, wave number, and impedance , we use the results of [24]. The numerical calculation was developed accordingly.

3.3.2 Corrections in the Evaluation of the Acoustic Pressure Variation in the Measurement Tube.

After examining the first measurement results, determined for quiet air, it was found that the reflections of the acoustic waves running in the tube and reflected at the microphones could not be disregarded. Even though the reflection factor on a microphone in measurement tube A, for example, is only 1000 Hz for $|r| \sim 4 \cdot 10^{-3}$, the individual contributions add up to a substantial change in the reflection factor r_{Ek}. A simple calculation of the impedance of the pressure taps ahead of the microphones using the wall conduction value for the viscosity and heat conduction wave was done according to Cremer [29]. It was not possible for it to completely eliminate the deviations between the measured and the theoretical reflection factors r_{Ek}. Therefore, the impedance of the microphones was calculated just like in [28]. There the reflection factor for the microphones was derived from the acoustic field ahead of the microphone membrane and in the pressure tap. The formulas found with this reflection factor and corrected for the influence of the microphones on the acoustic field in the tube can be corrected in the appendix. /14

3.3.3 End correction of investigated openings for air at rest.

As already mentioned in the introduction, in order to consider the air particles which oscillate near the opening, it is necessary to increase the actual length of the tube by $l_{Ek} = 0.85\ a$. For measurement

tube B, where the tube is closed off by a disc with the hole and the tube diameter is 20 mm, the conditions are somewhat different. In order to be able to take over the evaluation programs for measurement configuration A without substantial modifications, we again determined the reflection factor in the final plane of the impedence measurement tube. When calculating the external end correction, the impedance of the opening throat and the impedance of the inner end correction must also be considered.

The inner end correction, according to Ingard, depends on the ratio of the opening diameter and the tube diameter [7], and on the distance between the opening and the back wall of the tube (1). In the case of /15
the measurement tube B, the back wall (i.e., the flow resistance) was not separated so far from the opening that its influence could be ingnored. For the inner end correction, we then obtain

$$l_{Ek_i} = 0.85\ a\ (1 - 1.25\ a/R_R) \text{ for } a/R_R < 0.4,$$

i.e.,

$$l_{Ek_i} = 0.64\ a \text{ for } a/R_R = 0.2.$$

(R_R is the radius of the measurement tube).

The impedance of the opening throat is determined using well-known formulas for the impedance for a short and open tube.

Ingard [7] investigated the case of two round and eccentrically situated openings in a tube (see Table 1, opening 4). Here, two effects superimpose. First of all, the end correction changes because the openings are no longer located on the axis of the tube but eccentric with respect to it. Also, there is a mutual influence of both openings. In the case of opening 4, we find a ratio of $b/R_R = 0.4$ (b = distance between opening and center of tube). From the figures of Ingard, and from an interpolation, we find that for $a/R_R = 0.2$ and $b/R_R = 0.4$, the result is

$$l_{Ek_i} = 0.35\ a$$

The interaction part is therefore equal to 0 for the selected value of $b/R_R = 0.4$.

For the case where the number of openings is greater than 2, (perforated plate), according to Fok, [30], one can calculate the decrease in the inner end correction. He gave the following function: /16

$$\Psi = (1 + a_1\xi + a_2\xi^2 + \ldots)^{-1}$$

where

$a_1 = -1{,}40925$	$a_7 = 0{,}03015$
$a_2 = 0$	$a_8 = -0{,}01641$
$a_3 = 0{,}33818$	$a_9 = 0{,}01729$
$a_4 = 0$	$a_{10} = -0{,}01248$
$a_5 = 0{,}06793$	$a_{11} = 0{,}01205$
$a_6 = -0{,}02287$	$a_{12} = -0{,}00985$

Here we have , where $a_{eff} = \sqrt{\frac{S_n}{\pi}}$.

s_n is the area which is occupied by the n openings of the perforated plate. σ is the ratio of the area of all openings, and the total area, and is also called the porosity. For the end correction, we have

$$l_{Ek_i} = \frac{0{,}85\ a}{\Psi} .$$

For $\xi = 0$, we have $\Psi = 1$, and therefore again $l_{Ek_i} = 0.85$ a. For $\xi = 1$, Ψ becomes infinite and therefore $l_{Ek_i} = 0$. In the limiting case of many closely situated openings, the contribution of the individual openings vanishes. The end correction is then the one for the open tube.

(It should be noted that in the figures of [30] and [11], the function Ψ is correctly shown. However, in the formula, the reciprocal of Ψ is shown.) $\frac{a_{eff}}{a} = \sigma = \xi$

For opening 5 (9 openings) we therefore have

$$\Psi(0.6) = 4.32$$

and

$$l_{Ek_i} = 0.20\ a.$$

3.3.4 Examination of the Evaluation for Air at Rest /17

Using the formulas given in the last section for the end correction of the opening, it is now possible to calculate the theoretical reflection factor in the upper edge plane of the impedance measurement tube.

For example, for measurement configuration A, (almost soft sound termination of the tube) we find a reflection factor of

$$r_{Ek} = \frac{z_{Ek} - z_{Rohr}}{z_{Ek} + z_{Rohr}} \approx \frac{0{,}85\ a\omega i - \sigma c}{0{,}85\ a\omega i + \sigma c} \approx -1 + 1{,}7\ \frac{a\omega}{c}\ i$$

in other words, the real part is approximately -1 and the imaginary part is small and positive.

The average statistical error in the reflection factor according to the equalization calculation is about 0.4%. Figure 4 shows the difference between the theoretical and the measured values as a function of frequency. It is found that the deviations are of the same order, i.e., 0.5% of the magnitude of the reflection factor. The magnitude of the reflection factor is measured too small by 0.3% on the average.

The error in the reflection factor then leads to errors of different sizes in the calculation of the impedance of the end correction. We have

$$dz_{Ek} = \frac{2 \cdot z_{Rohr}}{(1 - r_{Ek})^2} dr_{Ek}$$

i.e., for a reflection factor with a small imaginary part and a real part about -1, (apparatus A) the inaccuracy in the reflection factor leads to a substantially smaller error in the impedance of the incorrection than is the case for a reflection factor with a real part of +1 and also a small imaginary part. Since this latter set of circumstances applies for apparatus B, (almost hard acoustic closure of the tube) there were large errors in the impedance measurements for that case, in spite of the same accuracy in the reflection factor. (If the /18
impedance of the end correction is changed by the tangential flow, then the conditions become more favorable).

In the further evaluation, the impedance of the end correction is always normalized using the imaginary part X_o of the theoretical value for air at rest. The normalized impedance for air at rest, therefore, has an imaginary part of $X/X_o = 1$, and a small positive real part R/X_o. Comparison with measurements shows the deviation of 5% at high frequencies, and of 20% for the frequency range around 200 Hz. On the average it is about 10%. In the case where the real part and the imaginary part of the impedance are greatly different, for example, for air at rest, (Im >> Re) for large flow velocities (Re << Im) a small phase rotation within the acoustic measurement instrumentation would lead to a large falsification of the smaller contribution. In order to exclude such errors, we also measured using an opening closed off with gauze. As was to be expected theoretically, the measurement shows that the imaginary part of the end correction does not change and the

increased acoustic resistance of the opening depends on frequency.

In the case of tangential flow, it is no longer possible to make a quantitative comparison with theory. Only the statistical error from the equalization calculation can be considered, which increases with turbulent flow. For example, the statistical error of the reflection factor for apparatus A is in general between 0.5% and 0.9% (maximum 1.5% for completely turbulent flow).

In the case of tangential flow tunnel, there is overpressure compared with the laboratory, and therefore additional error sources must be considered. The flow through the opening due to poor sealing /19
in the measurement tube or at the microphones can be excluded by testing the pressure drop in the closed-off tube as a function of time after each new installation. The change in the microphone sensitivity with static pressure is considered with the calibration.

4. Measurement of the Shear Layer Profile Above the Opening, Measurement Apparatus Set-Up, Execution of the Measurements and Evaluation.

The measurement of all the important parameters of the flow boundary layer of the opening represented a focal point for the investigations. A comparison of this data with the acoustic measurement results should show the influence of the boundary layer thickness, the shape of the boundary layer profile, and other parameters on the opening impedance. In order to measure the shear layer profile above the opening, we had available a hot-wire probe, which could be displaced in the vertical direction, a constant-temperature anemometer and a linearizer. From the shear layer profile, we determine the parameters required for the evaluation, such as the displacement thickness δ^*, the momentum loss thickness ϑ, the shape parameter $H = \delta^*/\vartheta$, the velocity gradient near the wall and the degree of turbulence. It should be realized that above the opening, the profile of the wall boundary layer is converted into a shear layer profile, which has a velocity different from zero within the opening throat. In order to determine the boundary layer thickness, a tangent was drawn at the inflection point of the profile, and then the profile of the wall boundary layer was reconstructed on the plate in front of the opening. The

recorder profiles differ with respect to boundary layer thickness (displacement thicknesses between 0.26 mm and 2.0 mm were measured) and with respect to shape. When the path lengths of the boundary layers /20
were different on the plate in front of the opening, we found profiles whose shape corresponded to the turbulent or the laminar plate boundary layer profile, as well as transitions between these. Figure 5 shows three different boundary layer profiles as examples. The flow velocity in these three profiles was the same and the displacement thicknesses were different. In order to be able to better identify the transition between the laminar and the turbulent profiles, we use the shape parameter H. For the turbulent boundary layer profile, we obtain H = 1.4 for the plate boundary layer, and H = 2.6 for the laminar one. [31]. For the boundary layers measured here, we found the values of H up to 3. This could be attributed to the fact that the calculation is based on the reconstructed profile of the wall boundary layer. In addition it was found that the boundary layer on the plate not always has the dependence in all cases, on the boundary layer thickness, path length, and incident velocity, as is predicted by theory. As mentioned in [31], the theoretical relationships hold exactly only for tunnels without a pressure gradient and low turbulence, which have carefully shaped plate leading edges. In these measurements, however, the velocity and pressure gradients were not corrected, which are caused by the fact that the boundary layer at the channel walls becomes thicker. The plate leading edges could only be made as pointed as was allowed by the channel geometry. The shape of the profiles corresponds to the shape of the plate boundary layer for laminar or turbulent flow, or for a transition state between them, as Figure 5 shows.

It is found that the measured and then normalized profiles can be represented to a good degree of approximation as the superposition of the laminar and turbulent plate boundary layer profiles.

$$\frac{y}{\delta^*}\left(\frac{u}{U}\right)_{exp} = \alpha \frac{y}{\delta^*}\left(\frac{u}{U}\right)_{lam} + (1-\alpha)\frac{y}{\delta^*}\left(\frac{u}{U}\right)_{turb}$$

Since we must expect that the influence of the flow on the opening impedance is essentially chracterized by the part of the profile near the wall, we characterize the measured profile by the velocity gradient γ at the wall. /21

$$\gamma \approx \frac{0,57}{\alpha}$$

As was expected, in the measurements we found a clear relationship with the shaped parameter H, and γ, so that we did not evaluate γ during the remainder of the evaluation. The laminar and turbulent character of the boundary layer profiles measured here can therefore be well-represented by H.

In order to vary the thickness and the shape of the boundary layer, the path length (plate length) was changed or tripping wires were attached ahead of the opening, and also the channel cross-section was changed. However, the attempts to produce thick laminar or thin turbulent boundary layers were not very successful. In order to show for what boundary layers the acoustic impedance and the uniform flow resistance of the opening could be determined, Figure 6 shows the quantities δ^* and H which characterize the boundary layer in these measurements. The measurements can be divided up into two regions. The first region is located at H = 1.5 (turbulent profile), and includes boundary layer thickness between 1 and 2 mm. All of the thinner boundary layers lie in the range. There, H takes on values between 1.8 and 3.

5. Measurement of the Uniform Flow, Resistance of the Opening with Tangential Flow. Design of the Measurement Installation, Measurement Execution and Evaluation.

In the measurement of the acoustic impedance of an opening, both for flow through the opening and for tangential flow, it is found to be appropriate to extrapolate the real part of the acoustic impedance to the frequency $\omega = 0$, and to then compare it with the uniform flow resistance of the opening. The purpose of this is to establish up to what frequencies the behavior of the acoustically-measured resistance of the opening can be characterized by the resistance measured for $\omega = 0$. If such relationships are found, it is possible to replace the complex acoustic measurements by simpler uniform flow measurements, at least for the low frequency range. /22

In order to obtain an overview on this, at the beginning of the acoustic measurements, and to determine how the uniform flow resistance depends on the flow parameters, we determined the uniform flow resistance for various shear layers. The same was done in almost all of the acoustic measurements, in order to be able to make the compari-

son discussed above. It was a disadvantage that both measurements could not be done simultaneously, but that instead the measurement instrumentation had to be rebuilt to measure the flow resistance. Instead of loudspaker 1, the measurement tube was closed off with a plate; the leads for compressed air and the measurement of the static pressure were contained in it. All of the installations in the tunnel were left alone. This conversion, unfortunately, had to be done because a tap for the measurement of the static pressure inside the impedance measurement tube would have represented an acoustic "leak", which could not have been considered in the exact calculation of sound propagation in the tube at the required accuracy.

In order to measure the uniform flow resistance, the pressure difference between the static pressure and the channel and in the tube is measured with a Betz manometer. Pressure changes down to 0.02 mmWS (water column, corresponds to 0.2 N/m^2) can be read off well. The average flow velocity through the opening is measured with a flux meter. The flow velocity v_G through the opening was a maximum of 40 cm/s, and therefore is on the same order as the speed of sound through the opening. For configuration A, it was a maximum of 30-40 cm/s, and for configuration B it was a maximum of 80 cm/s. The pressure difference between both sides of the opening plotted as a function of the flow velocity shows a linear relationship (Figure 7a). That means that in this range, the flow resistance is constant. /23

In [17, 18], it was reported that the flow resistances are discontinuous at v_G = 0 m/s. Depending on whether one comes from the side of positive or negative flow, one obtains flow resistance values which are different by more than 20% [18]. Since in our measurements, the flow velocities, the opening radius, and the ratio δ^*/a for the most part were in this same range, we were not able to detect this continuity. On the other hand, if from Figure 8 in [18], one calculates the relationship between the pressure difference and v_G, and we can see that a straight line results there as well.(constant flow resistance). The reason for the discontinuity is the fact that the line does not go through the origin, in other words, there were differences in the static pressure between the inside and the outside in the measurements, even without the flow (through the opening). This zero point displacement must be subtracted from the measured pressure

because the pressure taps in the channel and behind the opening react differently to the tangential flow.

The asymmetry of the uniform flow resistance found in [17] at high flow velocities (through the opening) is quite understandable, as discussed in the introduction. It occurs at v_G/U ratios which do not occur in our own experiments.

The inclinations of the lines in Figure 7a increased as a function of the flow velocity in the tunnel, i.e., the uniform flow resistance is a function of U. Figure 7b shows the uniform flow resistances for different flow velocities, and the boundary layer thickness did not change by more than 15%. This results in a linear relationship between R_S and U. However, this was no longer the case for the measurements where the boundary layer thickness changed drastically. As the boundary layer became thicker, R_S decreased in spite of increasing flow velocity. /24

In the following, we will consider only the additional uniform flow resistance R_G caused by the tangential flow. This is the resistance which results from the resistance R_S measured with tangential flow by subtracting out the resistance R_o obtained for quiet air.

$$R_G = R_S - R_o$$

This uniform flow resistance depends on the thickness of the boundary layer above the opening. In [14], we normalize the uniform flow resistance as follows:

$$A_{stat} = \frac{R_G}{\rho c} \cdot \frac{c}{0,85} \cdot \frac{1}{U}$$

(The reason for the special standardization of R_G will become clear in the comparison of the acoustic measurements of section 6.2.1). It was found that A_{stat} is a function of the ratio of the boundary layer thickness and the opening radius (δ^*/a). For the measurement configuration A and the opening radius a = 2 mm, Figure 8 shows the relationship between A_{stat} and δ^*/a found from the measurements. In the range $\delta^*/a \gtrsim 0.5$, A_{stat} is constant and has a value of $A_{stat} \sim 0.2$. For $\delta^*/a < 0.5$, A_{stat} increases. At $\delta^*/a = 0.15$, we find a A_{stat} about 0.65.

6. Measurement Results

6.1 Standardization of the Acoustic Impedance of the End Correction

In practice, in most cases, the flow properties of a tunnel are specified by its geometry and the installations which are installed once. If the installations are not changed, then one can specify the other parameters of the flow by specifying the flow velocity. For example, the boundary layer thickness can be specified. The change in /25
the acoustic impedance of the wall linings, such as openings in the channel wall, is therefore usually considered in these cases as a function of the flow velocity. As an example, Figure 9 shows the acoustic impedance of the end correction of an opening as a function of the flow velocity in the complex impedance plane. The real and imaginary part are made non-dimensional with ρc. In the following, we will first consider the solid line parts of the measured curves. We will discuss the dashed parts later on.

One can see the characteristic properties of the impedance curve as discussed in [14].

1. For small flow velocities, the impedance describes a spiral in the complex plane.

2. For large flow velocities, this spiral becomes a straight line. This range is called quasi-stationary, because here the stay time of the flowing fluid over the opening is small compared with the acoustic period.

From the individual representations for the real part and the imaginary part, we can see the following.

3. In the spiral range, the real part of the impedance end correction can become negative.

4. For large flow velocities, the real part increases linearly with U. (however, this only applies as long as the boundary layer thickness is almost constant).

5. The mass part of the impedance first increases above the value for air at rest.

6. For large flow velocities, the imaginary part decreases greatly. This decrease can be greater than the mass part of the end correction for air at rest. For the measurement shown in Figure 9, we found only 90% of the theoretical value of the imaginary part for air at rest. These characteristics in the impedance curve occurred for all the /26

measurements, with the exception of the spiral which usually was less well developed.

In the representation of the real part of the acoustic impedance, as a function of the flow velocity, we also show the uniform flow resistance R_G measured for the same conditions. It can be seen that the spiral with the uniform flow measurements cannot be covered. On the other hand, in the quasi-stationary range, the difference between the two curves becomes smaller with increasing tangential flow.(that is, with decreasing Strouhal number, see below). In other words, for large velocities the acoustic resistance approaches the uniform flow resistance.

At the range of small frequencies ($\omega \to 0$) the acoustic resistance should also approach the uniform flow resistance. In order to compare both resistances, the frequency is used as a parameter in the measurements, and the curves for the real part of the impedance are extrapolated to $\omega = 0$.

Compared with the other possibility of using the flow velocity as the parameter for the measurement, this has the advantage of the flow velocity and the other properties of the flow over the opening remain constant during the test series. If the boundary layer thickness changes during a measurement series, then deviations can occur in the curve discussed above. In our own measurements, because of the different installations in the tunnel, the boundary layer thickness no longer decreased with the flow velocity, but instead increased. This was associated with a decrease in the real part of the impedance, and a strong increase in the mass contribution (dashed variation, Figure 9). In section 6.2.2 we will show that in comparison with measurements for boundary layers of different thickness, the boundary layer thickness is responsible for the defects. Therefore, in all of the other measurement series, the frequency was varied and the flow velocity over the opening remained constant. As already discussed in section 3.3.4, the impedance of the /27 end correction was standardized with the imaginary part X_o of the impedance for air at rest ($X_o \sim 0.85\, a\rho\omega$). The frequency was made dimensionless with the flow velocity and the opening radius, and in this way one obtains a reciprocal Strouhal number, $S^{-1} = U/a\omega$. This standardization was also carried out in Figure 9, on the right and upper edge of the figure.

Figure 10 shows an impedance curve measured for constant boundary layer thickness. The properties of the impedance curve discussed above become apparent here as well. The measurement series was used for comparison to again clearly show the spiral. The quasi-stationary range with the linear connection between S^{-1} and the real part is not completely achieved in this representation.

6.2 Measurement Configuation A

In the following we will first discuss the results obtained with the measurement tube A. All of the results in this section were obtained with opening 1. The opening was made up of an 11-cm long and straight tube with a diameter of 4 mm which ends in the plate with the flow. By changing the flow velocity, the plate length in front of the opening, and by adjusting the wing at the trailing edge of the plate, different boundary layers over the opening resulted. Differences in the impedance of the end correction between the individual measurement series should be attributed only to influences of the tangential flow for this configuration. The flow should no longer have an influence over the sound propagation inside the tube, except in the opening region.

For 27 measurement series, we change the frequency in the range with /28
166 Hz up to maximum of 3000 Hz. The velocities of the channel flow varied between U = 4 m/s and U = 78.6 m/s. From this, we have the Strouhal number range $0.026 < S < 37.6$, and a reciprocal Strouhal number range of $0.1 < S^{-1} < 9.4$. For the displacement thickness, we had values between $\delta^* = 0.26$ mm and $\delta^* = 2.0$ mm. The shape parameter H was between 1.4 and 3. (The values of H and δ^* for the acoustic measurements were indicated in Figure 6 with squares). The results of these measurements are shown in Figure 11.

Since apparently the resistance and mass part of the impedance vary with S^{-1} in different ways, we will consider them separately in the following.

6.2.1 Real Part of the Opening Impedance

In the upper part of Figure 11, we show the real part of the impedance of the end correction as a function of S^{-1}. For five different boundary layer thicknesses, we show the points connected which belong to one

measurement series (constant U, variable frequency). For large S^{-1}, the measurement points lie quite well along a straight line, which has the equation

$$\frac{R}{X_o} = \frac{R}{0,85\ a\rho\omega} = A_{akust}\ S^{-1} + B$$

$$= A_{akust}\ \frac{U}{a\omega} + B$$

[14]. The inclination of this line apparently increases as the boundary layer becomes thinner. If one standardizes the real part of the acoustic impedance using ρc, then after a calculation we find

$$\frac{R}{\rho c} = 0,85\ A_{akust}\ \frac{U}{c}\left(1 + \frac{B}{A_{akust}}\ \frac{a\omega}{U}\right) \qquad /29$$

If ω goes to zero, then we obtain

$$\frac{R_{(\omega=o)}}{\rho c} = 0,85\ A_{akust} \cdot \frac{U}{c}$$

The line inclination

$$A_{akust} = \frac{R_{(\omega=o)}}{\rho c} \cdot \frac{c}{0,85} \cdot \frac{1}{U}$$

determined from the acoustic impedance can be compared with the standardized uniform flow resistance

$$A_{stat} = \frac{R_G}{\rho c} \cdot \frac{c}{0,85} \cdot \frac{1}{U}$$

discussed in section 5, because both were measured with the same conditions (Figure 12). First we will only consider the points indicated with circles (measurement configuration, A).

In [14], it was shown that A_{akust} and A_{stat} coincide for thin boundary layers. This can be verified from these measurements for δ^* up to 2 mm. The differences which still exist can be attributed to the fact that the acoustic measurement and the uniform flow measurement were performed separately (see section 5). If one also includes the measurement results using measurement configuration B, as a preliminary discussion to section 6.3, (Figure 12), squares), then the Figure gives an impression of how much it is possible to determine the inclination mentioned above using flow measurements.

The relationship between A_{stat} and δ^*/a discussed in section 5 should also hold for A_{akust} and δ^*/a according to the above. In Figure 13 we show the values of A determined from uniform flow measurements and from impedance measurements. As would be expected, these curves /30 lie quite well along a straight line. The scatter in the range

$\delta^*/a \leq 0.4$ is too large to be explained by the measurement inaccuracies, therefore one can raise the question of whether A depends on other parameters. Therefore, Figure 13b gives the relationship between A and the momentum loss thickness ϑ of the boundary layer. The shape of the curve remains the same. The scatter is not reduced. It seems to be somewhat smaller, but the changed scale must be considered. If one orders the measured points plotted against δ^*/a according to the shape parameter, then we have a slight change. Since the shape parameter H is the relationship between δ^* and ϑ, we should not expect a great influence on A according to the above. Since there are only sufficient measured values for the range $\delta^*/a \leq 0.4$ with different values of H, this range was shown in Figure 14 on an enlarged scale. Indeed, there is now a slight dependence on the shape parameter. The curves $A = f(\delta^*/a)$ are displaced to the left as H increases. The A apparently are determined by an effective flow velocity over the opening. This effective flow velocity could be understood as the weighted velocity distribution. The weighting function would have to decrease with increasing wall distance. The following discussion will demonstrate this.

First of all, the values of A become smaller with increasing boundary layer thickness, i.e., smaller flow velocity near the opening. However, they also become smaller when the effective flow velocity near the opening becomes smaller with increasing shape parameter H, that is, when the gradient γ of the standardized profile becomes smaller near the wall, assuming constant boundary layer thickness. Therefore, /31 we find that the ratio is best suited to characterize A, out of all of the other flow parameters.

It should be noted that we were not successful when we plotted A as a function of the boundary layer thickness formed with the inflection tangent of the boundary layer profile. The measured values scatter too much in this representation. Such a representation would be a measure for the non-standardized average inclination, in the lower range of the profile. According to [14], this should be the important parameter for thick boundary layers, and for $\delta^*/a \gg 1$ the A values should go to 0. However, in these measurements we found for $\delta^*/a \sim 1$ (opening diameter 4 mm) that the value of A was only about 0.2. This same value was found for $\delta^*/a \sim 2$ for uniform flow measurements with a 2 mm opening.

We could not determine whether this constant value is extended up to higher δ^*/a ratios.

In order to test whether the turbulent velocity fluctuations near the opening are responsible for the increase in the real part of the opening impedance, we measured the degree of turbulence at various points of the shear layer. However, we were not able to find any connection between the degree of turbulence and the inclination A.

In Figure 15 we attempted to show the most important relationships between the real part of the impedance and S^{-1}, as follows from the measured values of Figure 11. From the two figures we can see that the real part already increases strongly starting at $S^{-1} = 2$. The inclination of the curve is between 0.35 (thick boundary layers) and 0.85 (thin boundary layers). The curve of a real part bends off only for higher S^{-1} values, into the quasi-stationary line with an inclination between 0.2 and 0.6 according to the boundary layer thickness. As the boundary layer becomes thinner, the point of bending off is displaced towards larger reciprocal Strouhal numbers. The range of the steepest increase in the curve becomes larger. Assuming that this /32 trend continues towards smaller δ^*, we can expect a maximum A of about 0.85.

In order to determine the impedance of the end correction in the quasi-stationary region, we require not only the line inclination A but also the ordinate segment B. Therefore, from an extrapolation in the line in the quasi-stationary region, to $S^{-1} = 0$, we also determined B. However, we were not able to find a dependence between the flow parameters and B, as we could do for A. We could only establish that for thick boundary layers, we have $B \sim 0.5$, and for thin boundary layers, $B \sim 2$. However, in between we have B values of about -0.25 as well.

From the relationship given above,

$$\frac{R}{\rho c} = 0{,}85\ A\ \frac{U}{c}\left(1 + \frac{B}{A}\frac{a\omega}{U}\right)$$

and the standardization of the equilibrium flow resistance,

$$\frac{R_G}{\rho c} = 0{,}85\ A\ \frac{U}{c}$$

in section 5 we obtain

$$\frac{R}{\rho c} = \frac{R_G}{\rho c}\left(1 + \frac{B}{A}\frac{a\omega}{U}\right).$$

The factor $\left(1 + \frac{B}{A}\frac{a\omega}{U}\right)$ therefore is the ratio of the uniform flow resistance of the opening and the real part of the acoustic impedance. For

large S^{-1} it goes to 0.

In these measurements the ratio B/A was between 5.3 and -0.8. The term B/A · S can therefore amount to up to 50% of the impedance for S^{-1} = 10 for example. Therefore, we cannot ignore it in general. /33

The inclination A was determined from the uniform flow measurements. For B, we can only make the general statements given above. Summarizing, we can say that the variation of the real part of the acoustic impedance in the quasi-stationary range cannot be derived from the uniform flow measurements in a satisfactory and quantitative way.

If we consider the curves for the real part in Figures 11 and 15, then they seem to be divided into three regions. Up to $S^{-1} \sim 2$, we can see the spiral. In this region, the real part coincides quite well with all measurement series, in this representation. The maximum of R/X_o is located at $S^{-1} \sim 0.8$, and the minimum at $S^{-1} \sim 1$. The negative real part therefore can be explained by the fact that at this Strouhal number, apparently energy is supplied from the channel flow to the acoustic field in the opening.

In the region of larger S^{-1}, we have the transition region where the inclination of the real part curve is greater than the quasi-stationary line. As the boundary layer becomes thicker, this increase becomes flatter.

The transition into the quasi-stationary range occurs at increasing reciprocal Strouhal numbers, as the boundary layer becomes thinner.

6.2.2 Imaginary part of the opening impedance.

For the imaginary part of the opening impedance, we can no longer make such detailed statements as for the real part. Again, we can distinguish between the spiral part and the quasi-stationary part (Figure 11). /34

At $S^{-1} \sim 0.8$, the imaginary part reaches a maximum of about 1.5 X_o. After this, depending on the boundary layer thickness, we have different curves [the relationships are somewhat more clear in Figure 16a, (U = 40.3 m/s), and in Figure 15, (below), which shows curves for 5 boundary layer thicknesses].

The value of X/X_o decreases by only about 1/2 a unit for a boundary layer thickness of about 2 mm. At higher reciprocal Strouhal numbers, there is then a second maximum of the imaginary part. It becomes clear

why there was a growth in the imaginary part with flow velocity in the measurement shown in Figure 9.

For the smallest measured boundary layer thickness $\delta^* = 0.26$ mm, the imaginary part drops down to about $-0.5\ X_o$ then remains constant up to $S^{-1} \sim 18$. For higher reciprocal Strouhal numbers, the mass part decreases in all curves (the smallest measured imaginary part was $X/X_o \sim -2$ and $S^{-1} = 32$).

We can explain the fact that the imaginary part becomes negative using the cover-like behavior of the shear layer for large S^{-1} as observed. This cover-like behavior results in a spring-like character of the impedance.

The relationship between the shape of the curve for the imaginary part and the boundary layer thickness cannot be easily described in a quantitative manner, as was possible for the line in the quasi-stationary range. Therefore, from the curve we selected two characteristics, and investigated their independence of δ^*/a (see Figure 15). First of all, we consider the height of the second maximum of the curves as well as the reciprocal Strouhal number, where the curves first deviated from the curve for the thinnest boundary layer. These relationships /35 are shown in Figures 16b and 16c.

In the range $\delta^*/a \sim 0.2$, these two characteristics of the imaginary part curves vary the most. This is also the range in which the inclination A of the real part of the impedance changes greatly.

6.3 Measurement Configuration B

In the measurements discussed in the previous chapter, the opening was 11 cm long, that is , the tube itself. However, this case does not occur in practice. In general the ratio of the opening lengths and opening diameter is 1 or smaller. However, when the opening ends in a cavity (here the wide tube with a diameter of 20 mm), then there will be additional defects which influence the impedance along the inner side of the opening or in the cavity. Therefore, we can ask to what extent the results obtained for the long opening can be transferred to these thinner openings.

6.3.1 Openings of Different Lengths

First of all, we measured two openings (diameter 4 mm) with a length

of 4 and 1 mm, using measurement configuration B. The measurements were carried out for both openings for the same boundary layer thickness. As an example, we show the curves for U = 69.8 m/s (Figure 17). In principle, we obtain the same results for the other flow velocities. We also show a measurement series for comparison (U = 69.8 m/s), which was recorded using measurement configuration A at approximately the same boundary layer thickness. /36

For the real part, we do not find any great differences between the 4-mm or the 1-mm opening length. In the case of the uniform measurements, we obtain approximately the same value for both openings (A ∿ 0.60 for $\delta^*/a \sim 0.34$). For the same δ^*/a ratio, a maximum value of A = 0.35 was measured using measurement configuration A. (Figure 13a). Therefore, the comparison curve (measurement configuration A) in the quasi-stationary range differs clearly from the curves for the two other thinner openings. The ordinate sections B are also different. We can notice differences in the imaginary part for the 4 mm and the 1 mm opening length. The curve for the 1 mm length runs at a distance of about one unit below the curve for the long opening (A). In the case of the 4 mm long opening, the mass loss is much larger in comparison, from about 1 X_o at $S^{-1} = 2$ to -2 X_o at $S^{-1} = 16$. The reasons for these differences can be attributed to the changes in the opening geometry and because of the presence of the cavity behind the opening.

For air at rest, the value for the impedance of the end correction of the opening was properly derived from the measurements; in other words, the correct value for the inner end correction was substituted in the data reduction.

When calculating the reflection factor along the top side of the measurement tube, it is assumed that the flow does not influence the acoustic field in the opening throat and the measurement tube. Certainly this is no longer the case for thin openings. Therefore, the measurement results are no longer to be interpreted as though they alone give the impedance of the end correction. Instead, the influences of processes behind the opening and in the cavity are also included. (vortices). These differences between the undisturbed sound propagation in the measurement tube for air at rest and disturbed sound propagation with tangential flow cannot be separated from the changes in the impedance in the end correction using this data reduction. However, it is questionable whether it is possible to separate the flow into two parts

in the opening region, where one is responsible for the change in the impedance of the outer end correction, and the other is responsible for the same for the inner end correction.

6.3.2 Two adjacent openings.

As the next item, we investigated two openings (diameter 4mm, length 4 mm) which were located symmetrically with respect to the axis of the measurement tube at a distance of 8 mm from each other.(σ = 0.08).

The inner end correction was assumed to be $l_{Ek_i} = 0.35$ a in the evaluation for the two openings (section 3.3.3). This value could not be immediately assumed for the outer end correction, because the openings could not emerge into a tube and instead emerged into a hemispherical space. As discussed in section 3.3, there should be a transition between the sum of the end corrections and several individual openings ($\sigma << 1$) and the one for the single tube ($\sigma = 1$) as a function for the number of openings.. In agreement with this, we find a somewhat greater end correction for each of the two adjacent openings which lie between 1.5 X_o and 1.1 X_o, and depend somewhat on frequency.

In the following figures, we show the impedance of the end correction of the individual opening. This is true for measurements using two or nine openings. We make the variable non-dimensional using the theoretical imaginary part ($X_o \sim 0.85\ a\rho\omega$) at rest. This means that we can compare the individual opening and several adjacent openings. The /38
measurements with tangential flow were performed for two different configurations of the openings with respect to the flow direction. In the first case the openings were behind each other in the flow direction. In the second case they were perpendicular to it. In this way, we wish to establish whether interactions between the two openings occurred because of the flow.

Figure 18 shows the measurement results compared with the individual openings (diameter 4 mm, length 4 mm.) The flow parameters, again, were U = 69.8 m/s and $\delta^*/a = 0.34$. The curves for the real part deviate somewhat from each other, but the deviation is small compared with the scatter of the measured values. In the case of the imaginary part, the mass decrease is almost equal, if we consider that the mass fraction of the end correction for the air at rest for two openings is

greater than for a single opening. The only exception to this is that after $S^{-1} = 10$, the imaginary part for openings perpendicular to the flow decreases drastically, in contrast to other curves.

Because of the similarity of the curves up to $S^{-1} = 10$, we can conclude that within the framework of the measurement accuracy, and a distance of 8 mm between the two openings, no interaction was caused by the tangential flow. This is true for openings parallel and perpenicular to the flow direction.

6.3.3 Nine Adjacent Openings

In order to be able to investigate the behavior of the acoustic impedance of a perforated plate in tangential flow, as using our instrmentation, we drilled nine holes in the exchangeable end discs of the measurement tube B. The diameter again was 4 mm ($\sigma = 0.36$, other dimensions given in Table 1). For air at rest, the imaginary part of the end correction of a single opening again was a value which is greater than X_o; as a function of frequency it was situated between 3.3 X_o and 2.2 X_o. The curves measured for tangential flow were again compared with those for the single opening. Figure 19 gives an example of the measurement for U = 69.8 m/s, $\delta^*/a = 0.34$. There are differences in the spiral region for the real part. On the other hand, the deviations between the quasi-stationary lines are not very great after $S^{-1} \sim 9$.

The imaginary part was measured for small S^{-1} up to 3.5 X_o. After this the curves are similar to those found for two openings and they are at about the same distance from one another. Above $S^{-1} > 14$, the mass part of the end correction of one of the nine openings decreases greatly compared with a single opening. At $S^{-1} \sim 22$, we reach a value of $-4\ X_o$. It could be that here the differences in behavior of the end correction of the 4 mm opening and the end correction of the measurement tube B (20 mm) become noticeable for tangential flow. The measurement results for the other tangential flow velocities are similar.

6.3.4. Opening with Rounded Edges

During the investigation of the single opening, we pose the question of the dependence of the opening impedance on the boundary layer thickness. We wish to establish how great the changes are caused by

different machining of the opening, for example, rounding off of the opening upper edge. All of the previously mentioned openings always /40
had sharp edges. One of the openings (diameter 4 mm, length 4 mm) had a greatly rounded off upper edge (rounding radius 1 mm, see Table 1). The calculation of the impedance of the end correction was done as though the opening throat was 4 mm long, in other words, the effects caused by the rounding off were contained in the end correction impedance. Therefore, for air at rest we only measured values between $0.5\ X_o$ and $0.8\ X_o$. In Figure 20 we again show the results for the measurements performed at U = 69.8 m/s and $\delta^*/a = 0.34$.

By rounding off, the increase in the lines in the quasi-stationary range becomes flatter (for the sharp edge opening, $A \sim 0.6$; for the rounded opening, $A \sim 0.4$). The fact that A has decreased by almost one-half is probably not to be interpreted as though the rounding makes the influence of the flow on the flow side end correction almost vanish.

In the spiral range the values for the rounded opening are also smaller. Just like for air at rest, in the case of tangential flow, the mass fraction of the opening impedance is smaller. However, this is only true for the spiral region, above $S^{-1} = 3$ all the curves are about the same; in other words, the rounding off does not have any great influence on the imaginary part. We can see that the rounding off of the opening edge on the side of the flow has a great influence on the real part of the impedance. In order to obtain a similar decrease from $A \sim 0.6$ to $A \sim 0.4$, for measurement tube A, for example, the boundary layer thickness would have had to increase by 50% there.

6.4 Comparison betwen Both Measurement Configurations. /41

As a conclusion, we will again compare measurement results obtained with measurement configuration B with those obtained with measurement configuration A.

For the real part, we can see that for constant boundary layer thickness, the inclination of the straight part of the curve was independent of the opening length (4 mm or 1mm), or of the number of openings. We found large differences for the inclination A, when the edges were rounded off, or between the measurement results for both measurement tubes. Figure 21 again shows the values measured with the long tube

$A = f(\delta^*/a)$. Also we show the A-value obtained from acoustic measurements and uniform flow measurements for openings of different lengths, for two or nine openings, and for the rounded opening. The differences between the measurement results with both configurations are greater than could be explained by the measurement accuracy. The A-value for the rounded off opening should be considered in connection with the results for measurement B. (The fact that they coincide with those for measurement configuration A is probably a coincidence.) The A values determined with measurement B (the acoustic as well as the static values) differ from those obtained with measurement tube A. Therefore, it must be assumed that the opening behind the cavity is responsible for this. In contrast to the imaginary part, apparently it does not matter whether the opening has a length of 4 mm or 1 mm.

For comparison we will again consider the A values obtained for uniform flow given in [15]. There, measurements were performed in a channel with strong pressure gradients for three different laminar boundary layers. Just like in our measurements, where only the boundary layer thickness was changed, the A values lie quite well along a curve (Figure 22a.). It is found that the A value from [15] coincides well with our own measurements with measurement tube A, even though in [15] there was a 80 cm^3 cavity behind the opening. /42
This seems to indicate that the strong pressure gradient given in [15] has an influence on A because of the form parameter. Unfortunately we cannot make additional statements, because in the measurements of [15] the boundary layer profile was not evaluated as accurately as in our measurements.

Previously, for the same boundary layer thickness we made measurements with different opening radii (opening length 4 mm, the 7 mm opening was 9.8 mm long). Figure 22b shows the result; the $A = f(\delta^*/a)$ curves are displaced to the right with decreasing opening radius. The changing ratio of the opening length and opening radius does not seem to be the reason why the measurements for the 7mm opening ($l/a = 2.8$) and the 3-mm opening ($l/a = 2.67$) are clearly separated from one another.

Not as much information can be obtained for the imaginary part for comparison between the various measurement configurations. In contrast to the real part, we find differences, not only between both measurement configurations but also for different opening lengths. The deviation

was not so great for two or nine openings, next to one another.

7. FINAL CONCLUSION /43

7.1 Measurement Results

In order to make general statements about the general behavior of the acoustic impedance of openings in a tangential flow, it is necessary to compare measurements where only one of the various parameters was varied.

First of all, we can state the following, and these statements are valid for all of the impedance curves measured for a constant boundary layer thickness. In the complex plane, the impedance of the end correction with tangential flow first describes a spiral with decreasing frequency, and then emerges into the so-called quasi-stationary region (Strouhal number goes to zero). There, the normalized real part can be described as a function of the reciprocal Strouhal number S^{-1} in the form of a straight line (in other words, the real part divided by ρc goes to a constant value). Inclination A of this straight line can be determined from the uniform flow resistance of the opening, which is suitably normalized. If we change the boundary layer thickness above the opening, then it is found that the inclination of the straight line for the real part is best represented as a function of the ratio of the displacement thickness δ^* and the opening radius a. The form parameter H of the boundary layer profiles only has a small influence. In other words, there are no large differences between the inclination of the real part measured for laminar or turbulent layer profiles, assuming that the displacement thickness δ^* is the same. For $\delta^*/a < 0.3$, A increases greatly (4 mm opening). The normalized imaginary part, as a /44 function of S^{-1}, also changes in the same region. For thin boundary layers, the imaginary part decreases until it takes on a constant value of about $-0.5\ X_o$ for large S^{-1}, that is, in the complex plane the impedance curve becomes a parallel line to the real axis. As the boundary layer becomes thicker, on the other hand, in the region $S^{-1} \sim 10$, a second maximum develops. The imaginary part remains positive. For very large S^{-1}, we find a further decrease in the mass fraction of the impedance for all measurements. The relationships given here appear especially clearly when the opening throat is very long (Apparatus A).

For the case where the opening is no longer formed by a tube with a constant diameter, but emerges into a larger tube after 4 or 1 mm, there are changes, even though the other parameters remain unchanged, especially the boundary layer thickness. The inclination of the straight line for the real part barely changes between the 4 mm opening and the 1 mm opening length. Both are clearly different compared with values measured with the long tube. There are clear deviations in the imaginary part already between the 4 mm and the 1 mm opening lengths. Both curves are different from those measured with the long tube.

If several openings emerge into the large tube and again for the same boundary layer thickness, then in these measurements the inclination of the real part of the impedance of the end correction (referred to one of the openings) is about the same as for the single opening. For the imaginary part curves, there are changes compared with the single opening only at large reciprocal Strouhal numbers. If the opening /45
edges are greatly rounded off, the inclination of the straight lines is reduced in the quasi-stationary range. The imaginary part is not influenced as much.

If one measures the uniform flow resistance for different opening radii with the same installations in the channel, then the curve mentioned above is displaced toward larger δ^*/a values. This curve gives the dependence of the inclination of the real part or of the suitably normalized uniform flow resistance on δ^*/a. These experimental findings can be classified as follows.

In the case of measurements with the long opening (measurement configuration A), the influence of the flow on the impedance of the external end correction was measured. Because of the evaluation with the reflection factor in the plane of the opening upper edge discussed here, there are other processes which contribute to the impedance of the end correction, which occur in the opening throat near the mouth.

On the other hand, if there is a cavity behind the opening as in measurement configuration B, then the additional influences on the impedance due to processes inside the cavity are carried along in the evaluation. These changes are the same for the real part of the impedance in the quasi-stationary range and the uniform flow resistance, compared with the measurement configuration A. They are independent of

the opening length for an opening length-to-opening radius ratio between 0.5 and 2. The variation of the imaginary part with S^{-1} is not only changed because of the cavity behind the opening, but also because of the different opening lengths.

7.2 Comparison of Measurement Results with Theory /46

Unfortunately, we can only make a qualitative comparison of the measurement results and the various theoretical models. This is because the theories mentioned at the beginning usually contain parameters which cannot be determined from measurements, or only with difficulty. Whether the assumptions for the models of openings in tangential flow are correct can therefore be better established by using the experiments for flow visualization over the opening.

The model of Ronneberger [14] which was developed for the case of small δ^*/a ratios, gives a correct qualitative variation of the impedance curve with the spiral and of the quasi-stationary range (linear increase of real part with S^{-1}, constant imaginary part) for thin boundary layers, as his measurements already showed. In the meantime, by means of flow visualizations above the opening, the most important assumptions of this theory have been confirmed. This model only includes processes which involve the interactions between the shear layer and the sound in the mouth region of the opening. The comparison of the measurement configuration with the long tube discussed in section 7.1 is appropriate here. For thin boundary layers, there is again a good qualitative agreement. It is only for large reciprocal Strouhal numbers that the imaginary part no longer remains constant in the measurements, but decreases further. The question of why this happens must remain open. The time delay between the sound pressure and the speed of sound over the opening should not be much greater for the impedance of the end correction than is the time which a air particle requires to cross the opening. It follows from this that the imaginary part of the impedance of the end correction should not decrease further, even though the real part increases linearly with S^{-1}. We cannot ex- /47
pect an explanation for the second maximum of the imaginary part which occurs for the thicker boundary layer from the model and its associated assumptions mentioned above.

The differences between the uniform flow measurements for openings with various radii can be explained as follows. After separation from

the leading edge of the opening, the plate boundary layer profile is converted into a shear layer profile. It is to be expected that the transition process of the shear layer will require different path lengths depending on the Reynolds number (formed with the momentum loss thickness). Such differences near the wall of the boundary layer profiles only have an influence on the properties of the opening impedance. This could be explained by the deviations between the two measurement configurations. It is conceivable that the turbulent velocity fluctuations in the opening depend on the impedance behind the opening (depending on the opening, there are different amounts of spring force). Another way to explain this, is to assume just like Mungur [21] that a vortex is created by the tangential flow in the cavity. For example, because of the tangential flow, there could be similar effects on both the internal end correction and the external end correction.

The possibilities presented here, unfortunately, are not capable of explaining the differences between the two measurement configurations and for the two different opening lengths.

In order to avoid speculation, and to form a basis for further theoretical work, it seems appropriate to investigate the question of the interaction between the shear layer over an opening (for example, in a Helmholtz resonator) and the speed of sound through the opening. This /48
should be combined with measurements of the acoustic impedance of the opening with flow visualization above the opening and in the cavity. In this way, effects which then occur during the measurement of the impedance can be directly related to influences of the tangential flow. Visual observation and simultaneous acoustic measurements should not be simple, however, especially for turbulent flows.

ACKNOWLEDGEMENT /49

I wish to acknowledge the support of Professor Dr. M. R. Schroeder, Director of the Third Physical Institute of the University of Goettingen, who made this work possible.

I wish to also thank Dr. Ronneberger for many discussions.

I wish to thank the members of the Third Physical Institute who supported me.

The evaluations of the measurement results were done on an H-632 computer, which was made available by the Volkswagen Foundation at the Third Physical Institute.

This work was done within the framework of the "Noise Production - Noise Elimination" task, supported by the German Research Community.

LITERATURE /50

1. U. Ingard; On the radiation of sound into a circular tube, with an application to resonators; J. Acoust. Soc., Am., 20, 665 (1948).

2. R. H. Bolt, S. Labate and U. Ingard; The acoustic reactance of small circular orifices; J. Acoust. Soc. Am, 21, 94, (1949).

3. G. B. Thurston; Periodic fluid flow through circular tubes, J. Acoust. Soc. Am., 24, 653 (1952).

4. G. B. Thurston, C. E. Martin; Periodic fluid flow through circular orifices; J. Acoust. Soc. Am. 25, 26 (1953).

5. A. W. Nolle; small-signal impedance of short tubes, J. Acoust. Soc. Am 25, 32 (1953).

6. G. B. Thurston, J. K. Wood; End corrections for a concentric circular orifice in a circular tube; J. Acoust. Soc. Am. 25, 861 (1953).

7. U. Ingard; On the theory and design of acoustic resonators, J. Acoust. Soc. Am. 25, 1037 (1953).

8. U. Ingard and S. Labate; Acoustic Circulation effects and the non-linear impedance of orifices, J. Acoust. Soc. Am. 22, 211 (1950)

9. G. B. Thurston, L. E. Hargrove, B. D. Cook; Nonlinear properties of circular orifices, J. Acoust. Soc. Am., 29, 992 (1957).

10. U. Ingard and H. Ising, Acoustic nonlinearity of an orifice, J. Acoust. Soc. Am. 42, 6 (1967)
J. Acoust. Soc. Am. 44, 1155 (1968) (letter)

11. T. H. Melling, The acoustic impedance of perforates at medium and high sound pressure levels, J. Sound. Vib, 29 1 (1973) /51

12. E. Feder, L. W. Dean; Analytical and experimental studies for predicting noise attnuation in acoustically treated ducts for turbofan engines, NASA CR-1373 (1969).

13. J. F. Groeneweg; Current understanding of Helmholtz resonator arrays as duct boundary conditions. NASA SP-207, 357 (1969).

14. D. Ronneberger; The acoustical impedance of holes in the wall of flow ducts. J. Sound Vib., 24, 133 (1972)

15. J. Kompenhans, D. Ronneberger; Experiments Concerning the flow dependent acoustic properties of perforated plates; AGARD conference Proceedings No. 131, Ref. 15 (1973).

16. P. D. Dean; An in situ method of wall acoustic impedance measurements in flow ducts; J. Sound Vib. 34, 97 (1974).

17. M. Budoff, W. E. Zorumski: Flow resistance of perforated plates in tangential flow. NASA TM X-2361 (1971).

18. T. Rogers and A. S. Hersh: The effect of grazing flow on the steady state resistance of square-edged orifices. AIAA 2nd Aero-Acoustic Conference, Paper 75-493, (1975).

19. K. J. Baumeister, E. J. Rice: Visual Study of the effect of grazing flow on the oscillatory flow in a resonator orifice, NASA TM X-3288 (1975).

---

20. D. Pohle: Visual investigation of acoustic flow in the vicinity of opening in tangential flow. Staatexamensarbeit, Drittes Physikalisches Institut, Goettingen (1976).

21. P. Mungur and J. L. Whitesides: Influence of Grazing Flow on duct wall normal impedances. AIAA 2nd Aero-Acoustics Conference, Paper 75-494 (1975).

22. E. J. Rice: A model for the Pressure excitation spectrum and acoustic impedance of sound adsorbers in the presence of grazing flow, AIAA Aero-Acoustics Conference, Paper 73-995 (1973).

23. I. B. Crandall; Theory of vibrating systems and sound, D. van Nostrand, New York (1926).

24. H. Tijdeman; On the propagation of sound waves in cylindrical tubes; J. Sound Vib. 39, 1 (1975).

25. A. S. Hersh and T. Rogers: Fluid mechanical model of the acoustic impedance of small orifices. AIAA 2nd Aero-Acoustics Conference, Paper 75-495 (1975).

26. E. J. Rice: A theoretical study of the acoustic impedance of orifices in the presence of a steady grazing flow. NASA TM X-71903 (1976).

27. W. Moehring; On flows with vortex sheets and solid plates. Max-Planck-Institute for Stromungsforschung, Goettingen, Report 128 (1973).

28. D. Ronneberger: Exact measurement of acoustic damping and phase velocity in tubes with tangential flow, considering the interaction between the sound and the turbulence. Professor paper, Mathematical faculty, University of Goettingen (1975).

29. L. Cremer: The acoustic boundary layer of rigid walls. Archiv d. elektr. Ubertr. 2, 136 (1948).

30. V. A. Fok, S. N. Rachevkin: Dokl. Akad. Nauk SSSR 31, 9, (1941), in: A course of lectures on the theory of sound. Pergamon press, London (1963).

31. Schlichting: Boundary layer theory, G. Braun, publisher, Karlsruhe, (1958).

APPENDIX /54

Ratio of Acoustic Pressure of Waves Running Back and Forth in Individual Microphones in the Measurement Tube.

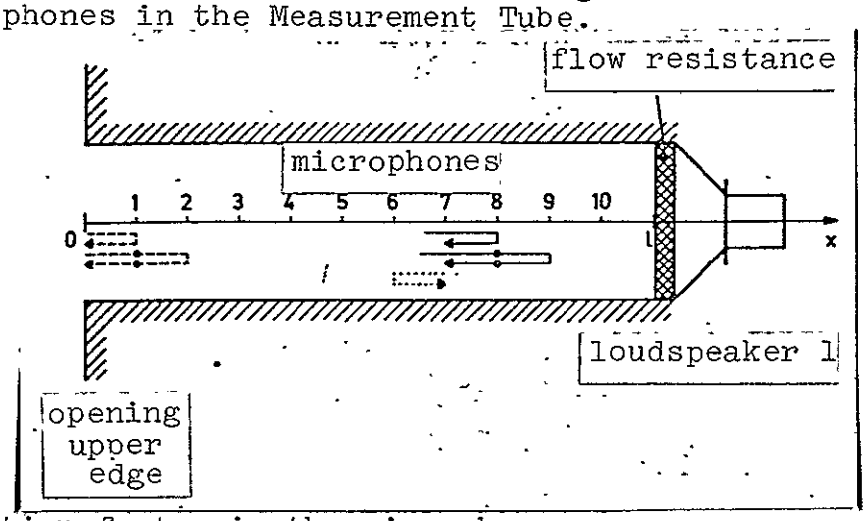

r reflection factor in the microphone

q reflection factor at the flow resistance

d microphone permeability factor

N number of microphones

x_n location of n-th microphone from the upper edge

r_{Ek} reflection factor in the plane of the opening upper edge.

1. Irradiation from Loudspeaker 1

1.1 Influence of microphones is not considered.

For x, we have:

$$p_1(x) = \hat{p}_{1+}\, e^{-ikx} + \hat{p}_{1-}\, e^{ikx}$$

for $x_o = 0$, we have /55

$$\hat{p}_{1+} = r_{Ek}\, \hat{p}_{1-}$$

It follows that

$$p_1(x) = \hat{p}_{1-} \left(r_{Ek}\, e^{-ikx} + e^{ikx} \right)$$

1.2 Influence of microphones on the sound pressure at the opening edge is considered.

The reflection factors for the microphones are very small. Therefore, we only have to consider the first reflections at the microphones.

If we consider the reflections indicated by dashed lines, then instead of the acoustic pressure $\hat{p}_{1+}$, we obtain the following acoustic pressure

at $x_o = 0$ for the outgoing wave:

$$p'_{1+} = \hat{p}_{1+}\left(1 + r\sum_{n=1}^{N} d^{2(n-1)}\, e^{-2ikx_n}\right) = r_{Ek}\,\hat{p}_{1-}$$

where

$$F_R = \left(1 + r\sum_{n=1}^{N} d^{2(n-1)}\, e^{-2ikx_n}\right)^{-1}$$

we have

$$p_1(x) = \hat{p}_{1-}\left(r_{Ek}\, F_R\, e^{-ikx} + e^{ikx}\right)$$

1.3 Influence of the N-1 microphones on the acoustic pressure in the in the n-th microphone.

For the n-th microphone, we have:

$$p_1(x_n) = \hat{p}_{1-}\Big[r_{Ek}\, F_R\, e^{-ikx_n}\, d^n\Big(1+r\sum_{\nu=n+1}^{N} e^{-2ik(x_\nu-x_n)}\, d^{2(\nu-n+1)}\Big)$$

(solid lines) /56

$$+\; e^{ikx_n}\, d^{(N-n+1)}\Big(1+r\sum_{\nu=1}^{n-1} e^{-2ik(x_n-x_\nu)}\, d^{2(n-\nu-1)}\Big)\Big]$$

(dotted lines)

where

$$C_n = d^n\Big(1 + r\sum_{\nu=n+1}^{N} e^{-2ik(x_\nu-x_n)}\, d^{2(\nu-n+1)}\Big)$$

and

$$D_n = d^{(N-n+1)}\Big(1 + r\sum_{\nu=1}^{n-1} e^{-2ik(x_n-x_\nu)}\, d^{2(n-\nu-1)}\Big)$$

we have

$$p_1(x_n) = \hat{p}_{1-}\left[r_{Ek}\, F_R \cdot C_n\, e^{-ikx_n} + D_n\, e^{ikx_n}\right]$$

2. Sound irradiation from the Outside

2.1 Influence of Microphones is not Considered.

For x, we have

$$p_2(x) = \hat{p}_{2+}\, e^{-ikx} + \hat{p}_{2-}\, e^{ikx}$$

for x = l we have

$$\hat{p}_{2-}\, e^{ikl} = q\,\hat{p}_{2+}\, e^{-ikl}$$

It follows that

$$p_2(x) = \hat{p}_{2+}\left(e^{-ikx} + q\, e^{-2ikl}\, e^{ikx}\right)$$

2.2 Influence of Microphones on the Sound Pressure Is Considered in the Flow Resistance. /57

For

$$F_Q = \left(1 + r \sum_{n=1}^{N} d^{2(n-1)}\, e^{2ikx_{N-n+1}}\, e^{-2ikl}\right)^{-1}$$

We obtain from a similar calculation, like 1.2

$$p_2(x) = \hat{p}_{2+}\left(e^{-ikx} + q\, e^{-2ikl}\, F_Q\, e^{ikx}\right)$$

2.3 Influence of the N-1 microphones on the acoustic pressure at the n-th microphone.

Just like in 1.3, we obtain

$$p_2(x_n) = \hat{p}_{2+}\left[C_n\, e^{-ikx_n} + q\, e^{-2ikl}\, F_Q \cdot D_n\, e^{ikx_n}\right]$$

We find the following for the acoustic pressure ratio at the location of the n-th microphone:

$$\frac{p_1(x_n)}{p_2(x_n)} = \frac{\hat{p}_{1-}}{\hat{p}_{2+}} \cdot \frac{r_{Ek}\, F_R\, C_n\, e^{-ikx_n} + D_n\, e^{ikx_n}}{C_n\, e^{-ikx_n} + D_n\, q\, e^{-2ikl} \cdot F_Q\, e^{ikx_n}}$$

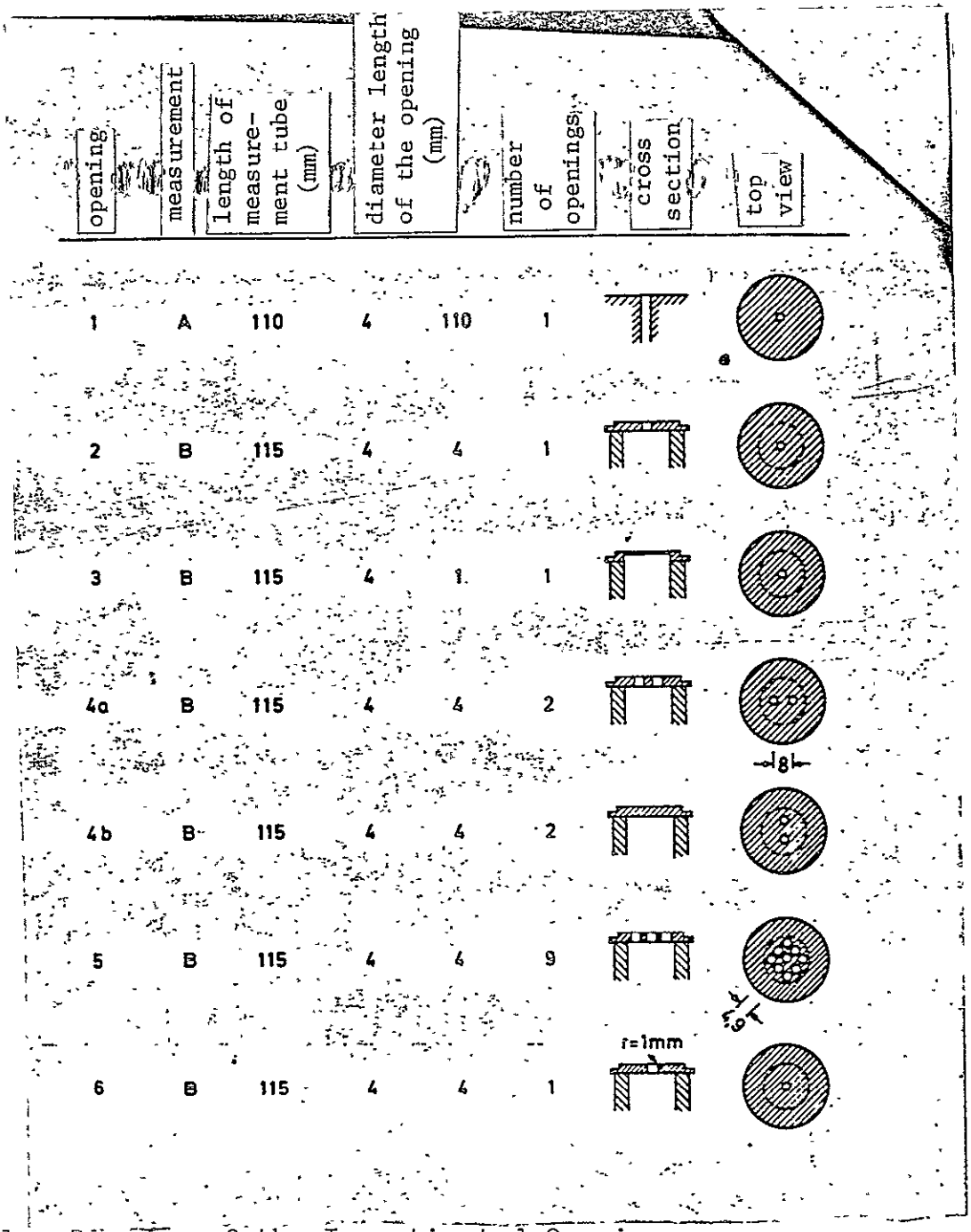

Table 1: Summary of the Investigated Openings.

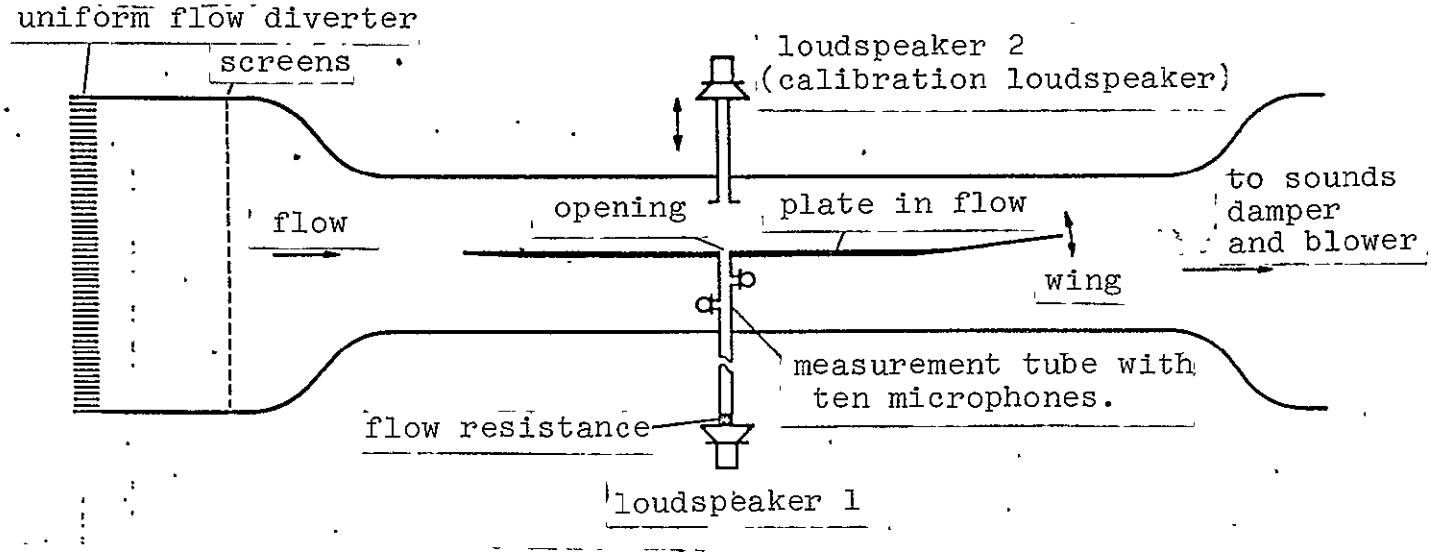

Figure 1: Sketch of measurement configuration (flow channel).

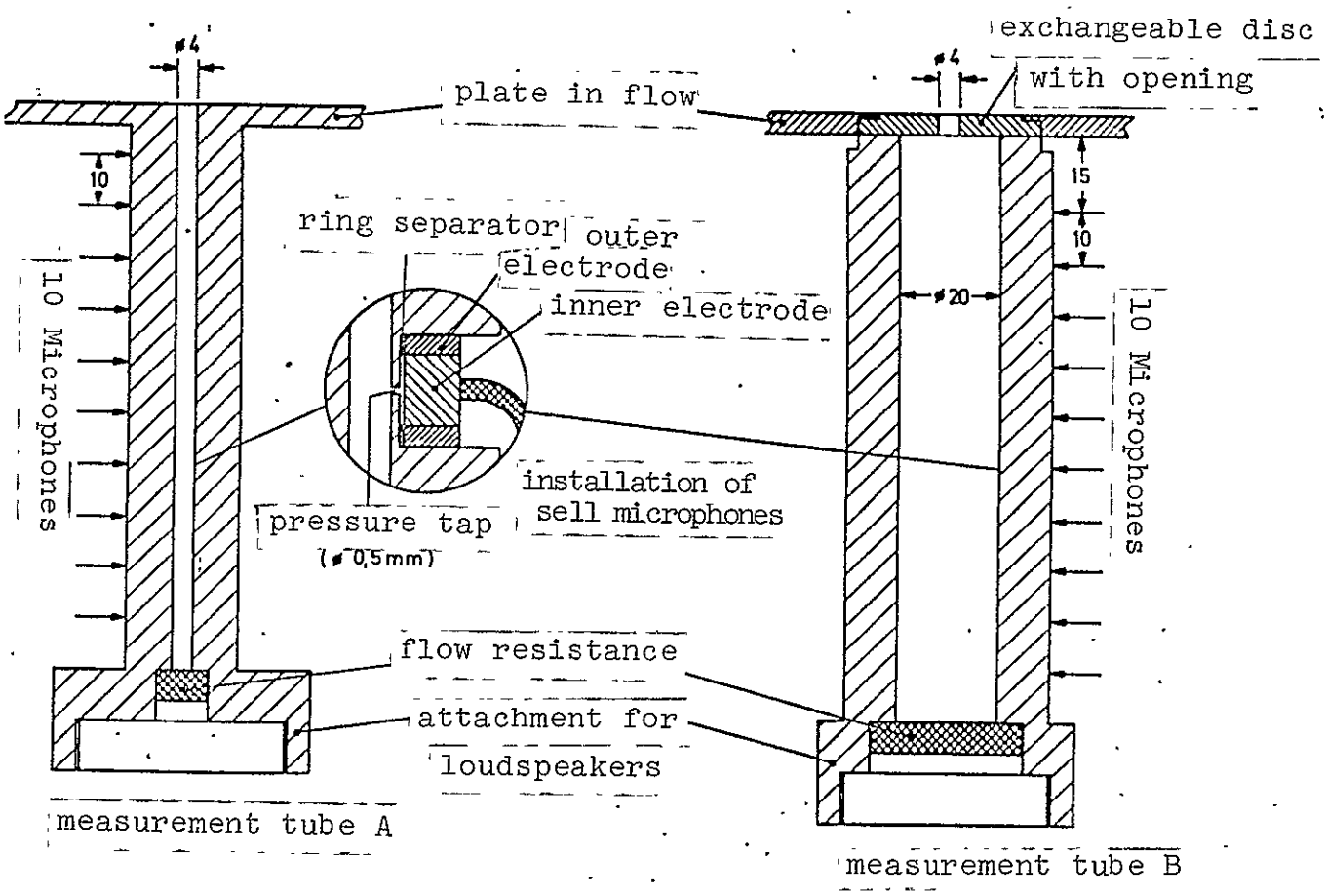

Figure 2: Sketches of the two measurement tubes and installation of the sell microphones.

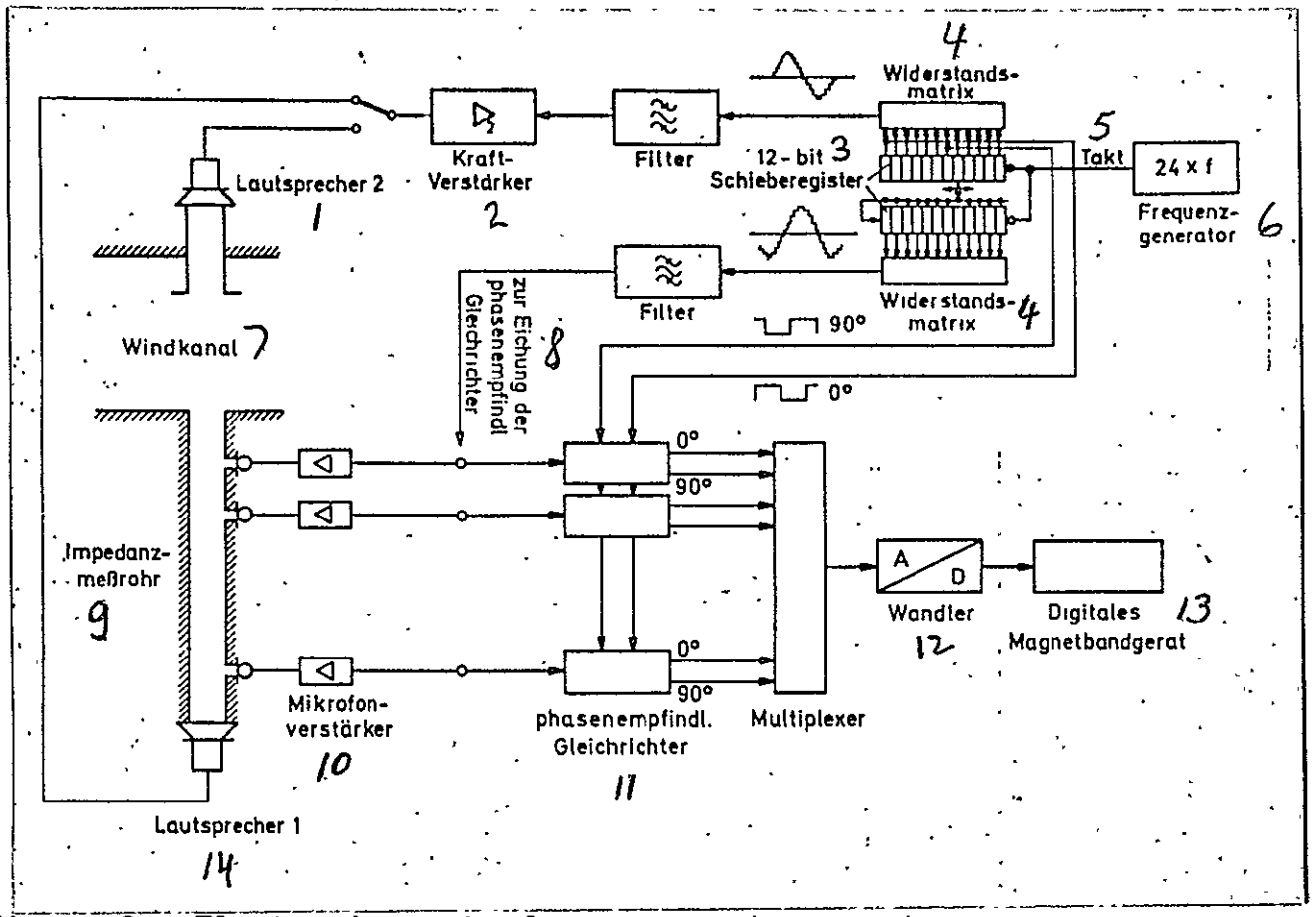

Figure 3: Electronic part of measurement apparatus.

1 - loudspeaker 2 2- force amplifier 3- 12-bit shift register 4- resistance matrix 5- timing pulse 6- frequency generator 7- wind tunnel 8- phase-sensitive rectifier for calibration 9- impedance measurement tube 10- microphone amplifier 11- phase-sensitive rectifier 12- converter 13- digital magnetic tape recorder 14- loudspeaker 1

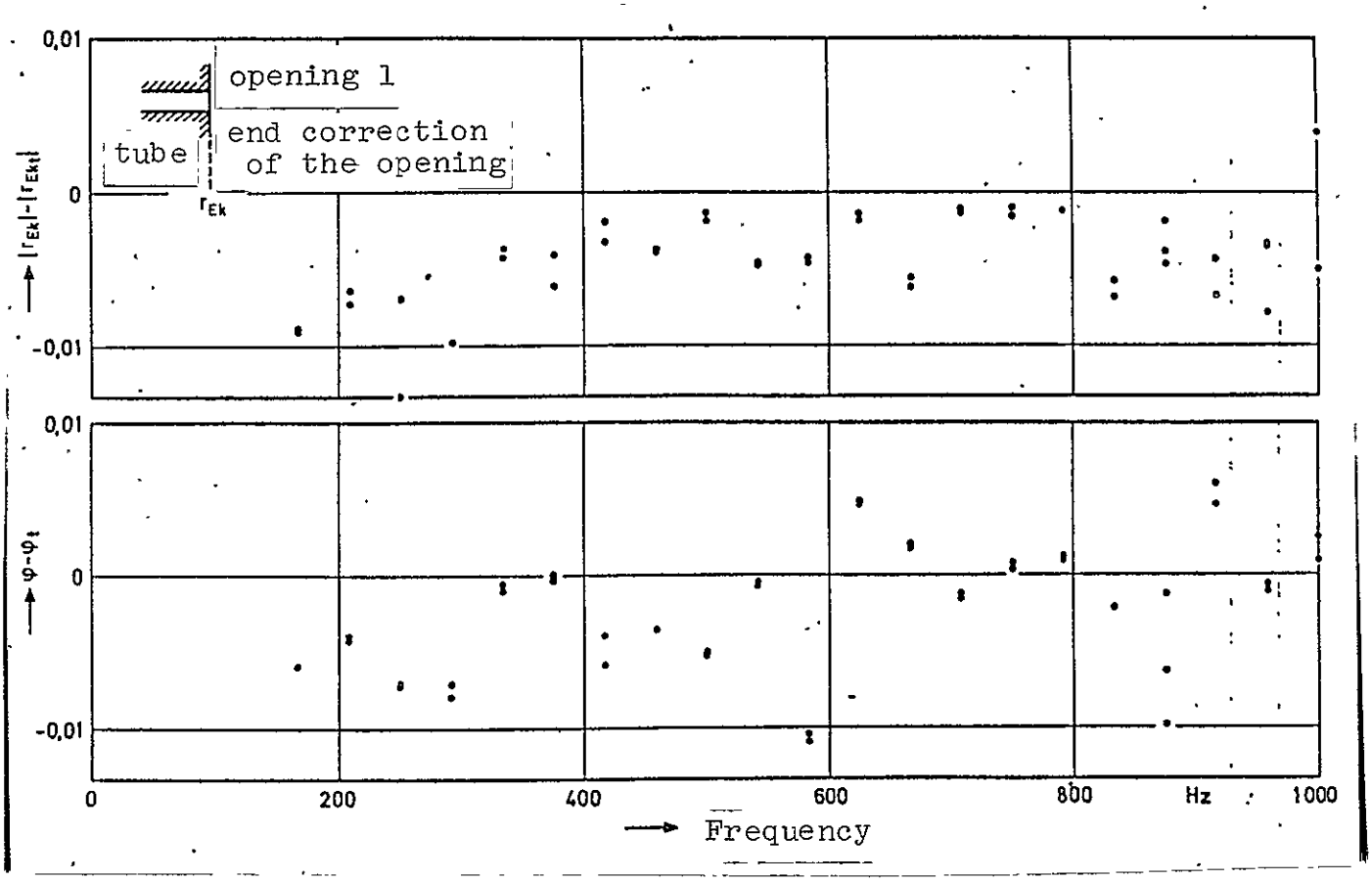

Figure 4: Difference between the measured and theoretical reflection factors in the plane of the opening upper edge, magnitude and phase (arc scale) ($a = 2$ mm, $|r_{Ek}| \sim 1$, $\phi \sim \pi$)

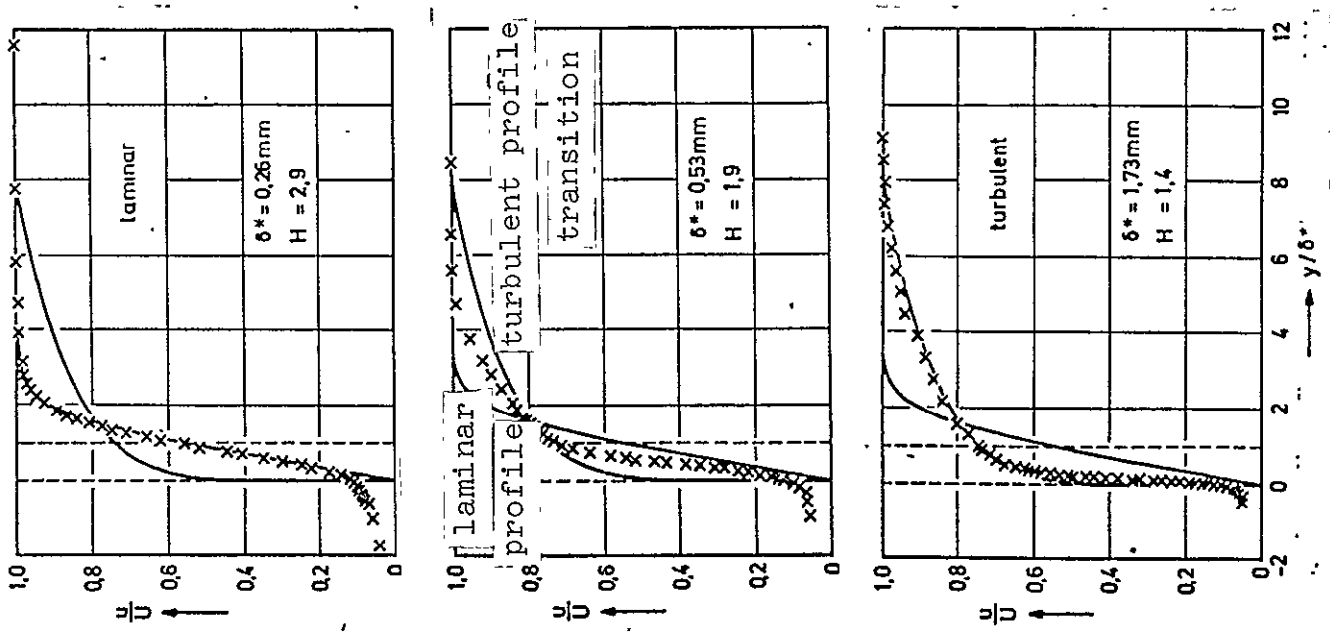

Figure 5: Various profiles of the shear layer over the opening (U = 49.4 m/s). For comparison, we show the theoretical plate boundary layer profiles of Blasius (laminar) and according to the 1/7 power law.

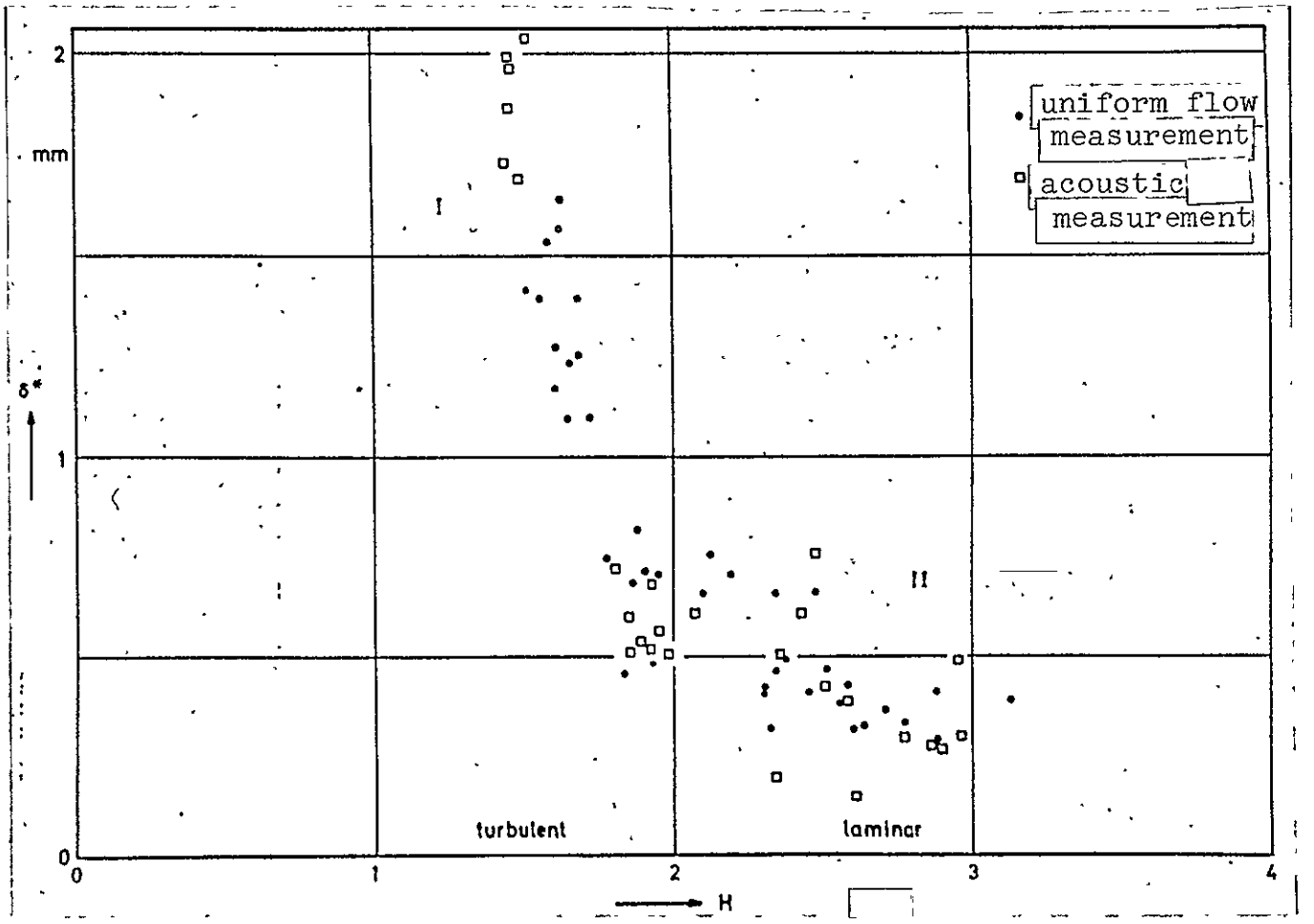

Figure 6: Form parameter H and boundary layer thickness δ* for measurements (uniform flow measurements were also made for u).

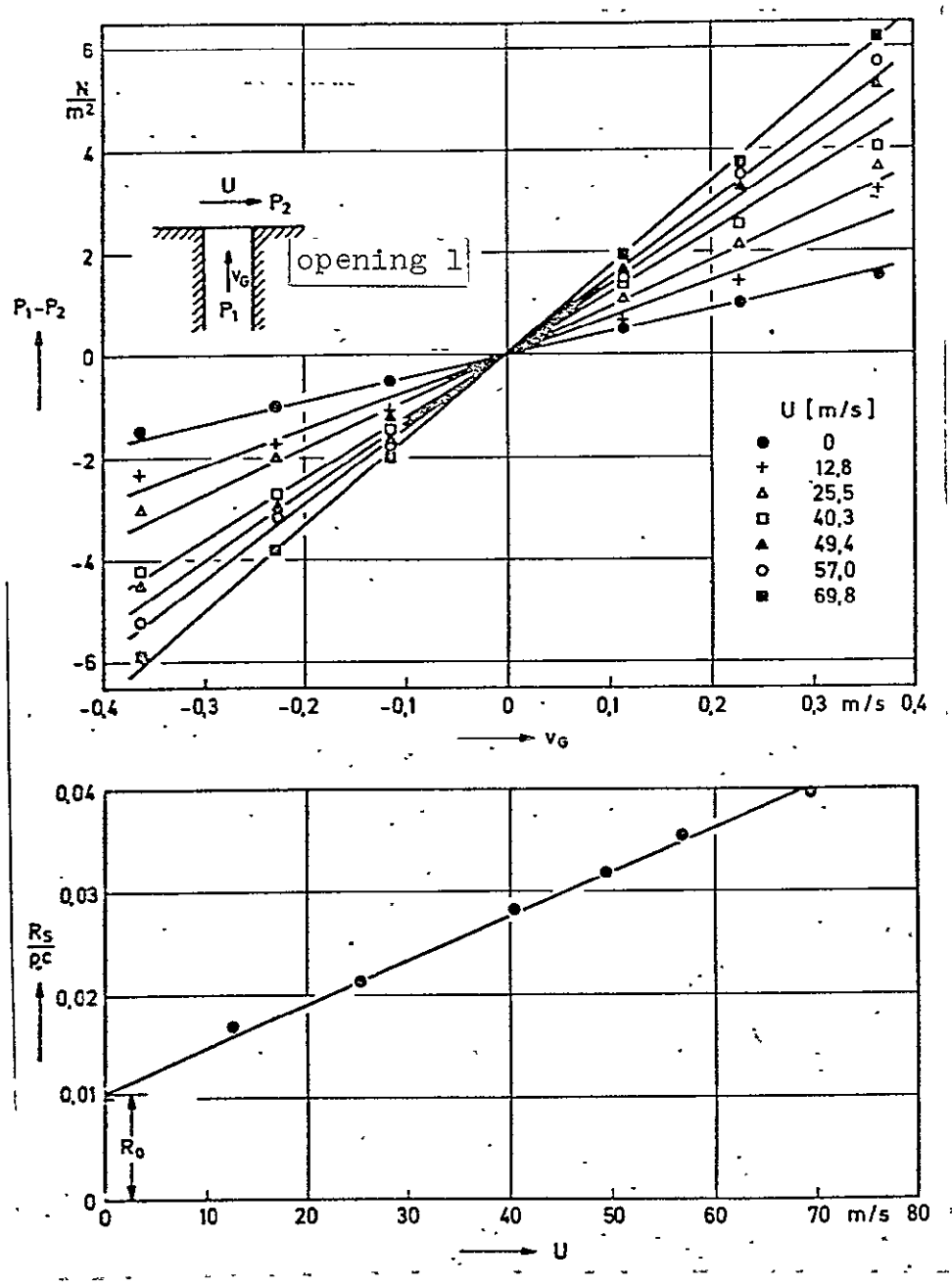

Figure 7a: Pressure difference between both sides of an opening (a = 2 mm) as a function of the flow velocity. The tangential flow velocity is the parameter (top).

7b: Uniform flow resistance of the same opening as a function of the tangential flow velocity ($\delta^* \sim 1.9$ mm.) (below)

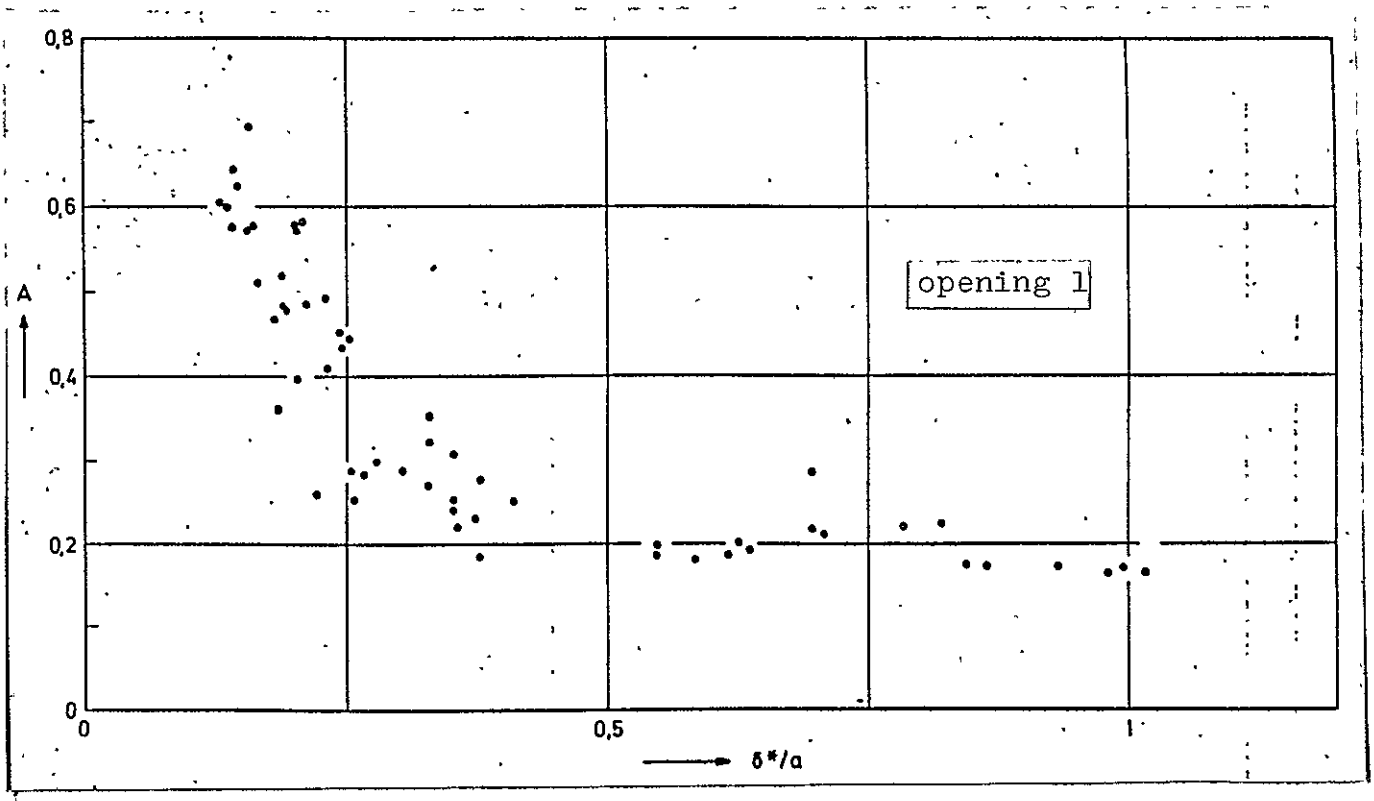

Figure 8: Normalized uniform flow resistance A of an opening (a = 2mm) measurement configuration A) as a function of boundary layer thickness δ* (see section 5 for standardization).

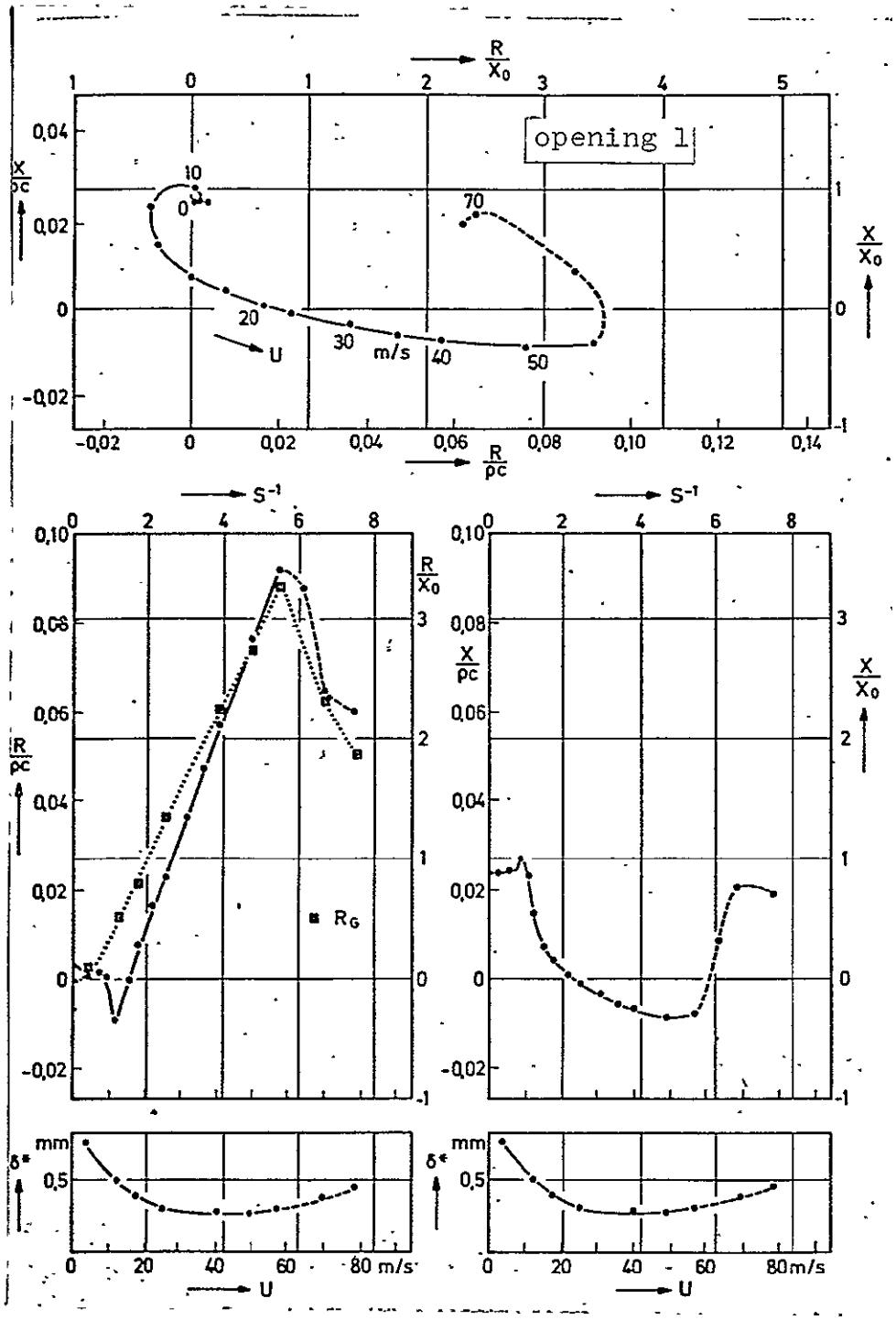

Figure 9: Impedance of the end correction of an opening (a = 2 mm) as a function of the flow velocity at f = 833 Hz. (▪: uniform flow resistance of opening).

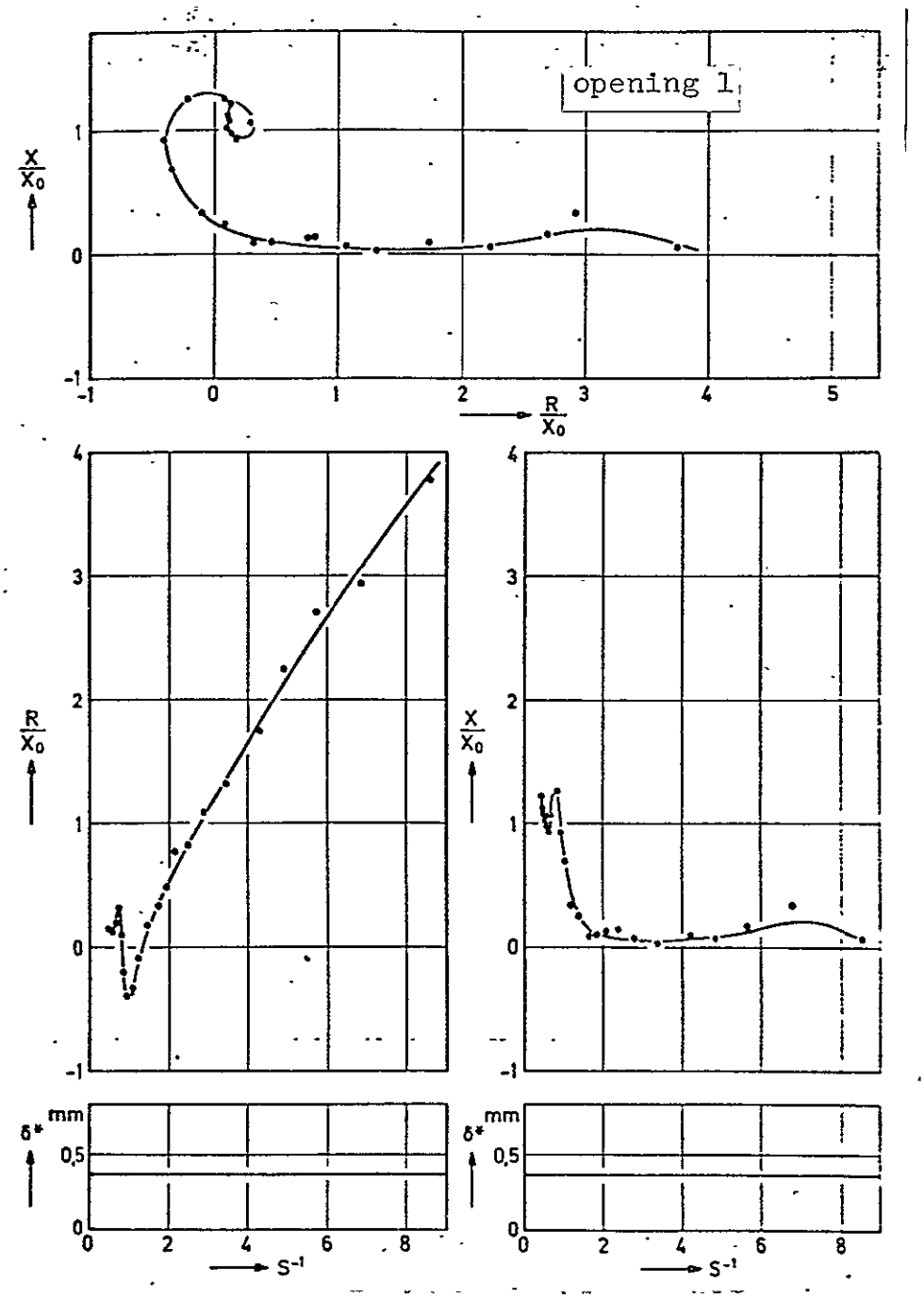

Figure 10: Impedance of end correction of an opening (a = 2 mm) as a function of reciprocal Strouhal number ($\delta^* = 0.38$ mm, U = 18 m/s).

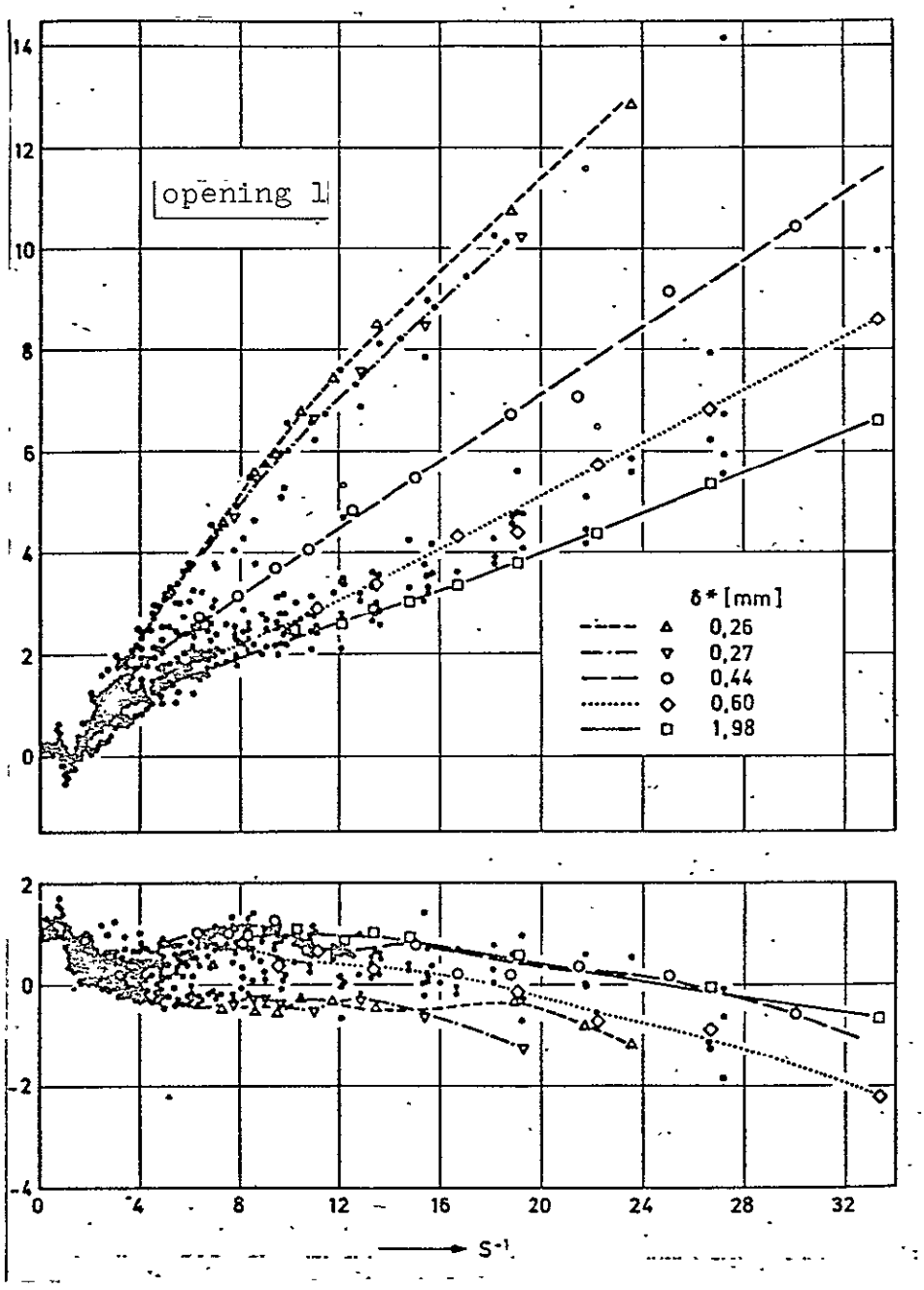

Figure 11: Real- and imaginary-part of the impedance of the end correction of an opening (a = 2 mm) for different boundary layer thicknesses.

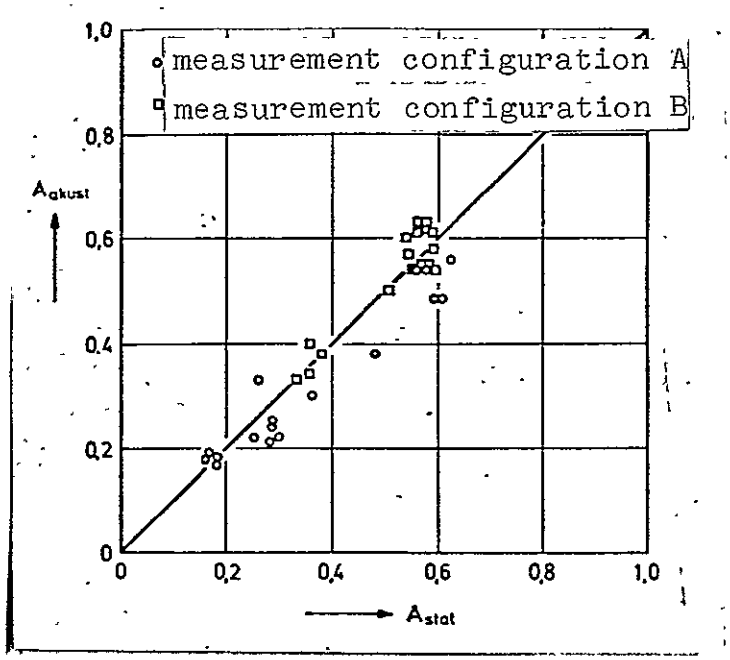

Figure 12: Comparison between the acoustic and the uniform flow measurements used to determine A.

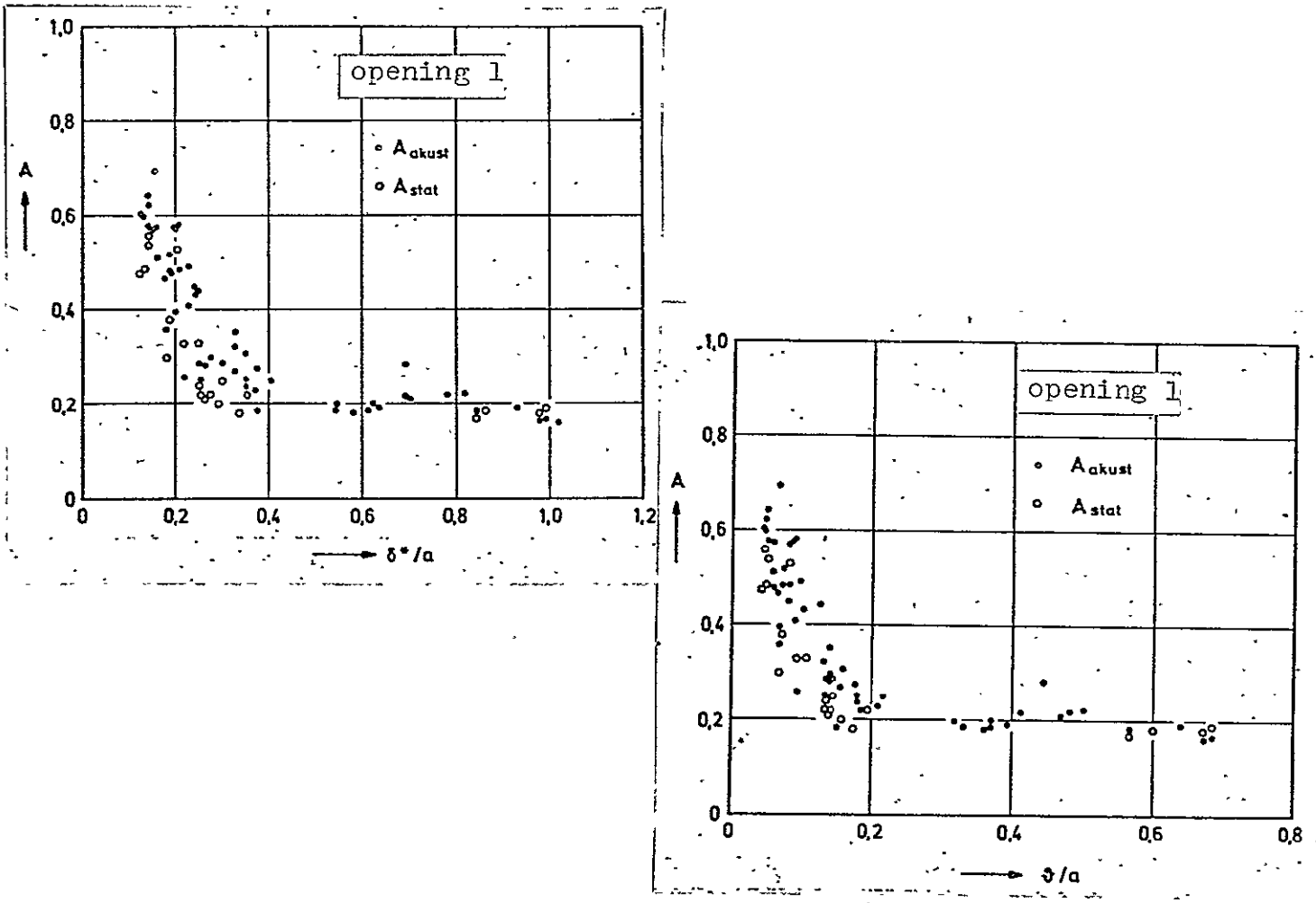

Figure 13: A is a function of boundary layer thickness.

a) as a function of displacement thickness δ^*, (top)
b) as a function of the momentum loss thickness ϑ (bottom)

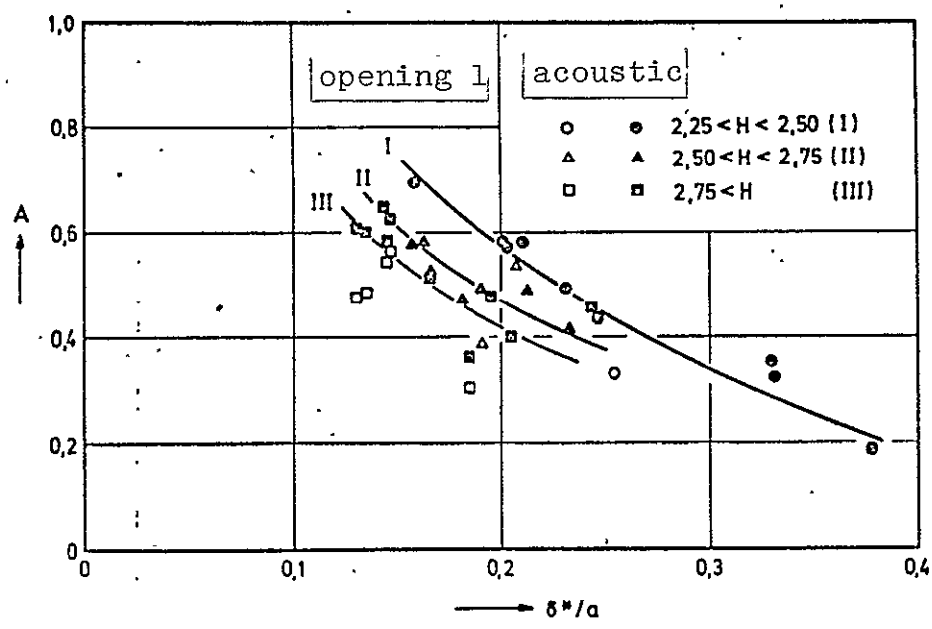

Figure 14: Influence of the form parameter H on A.

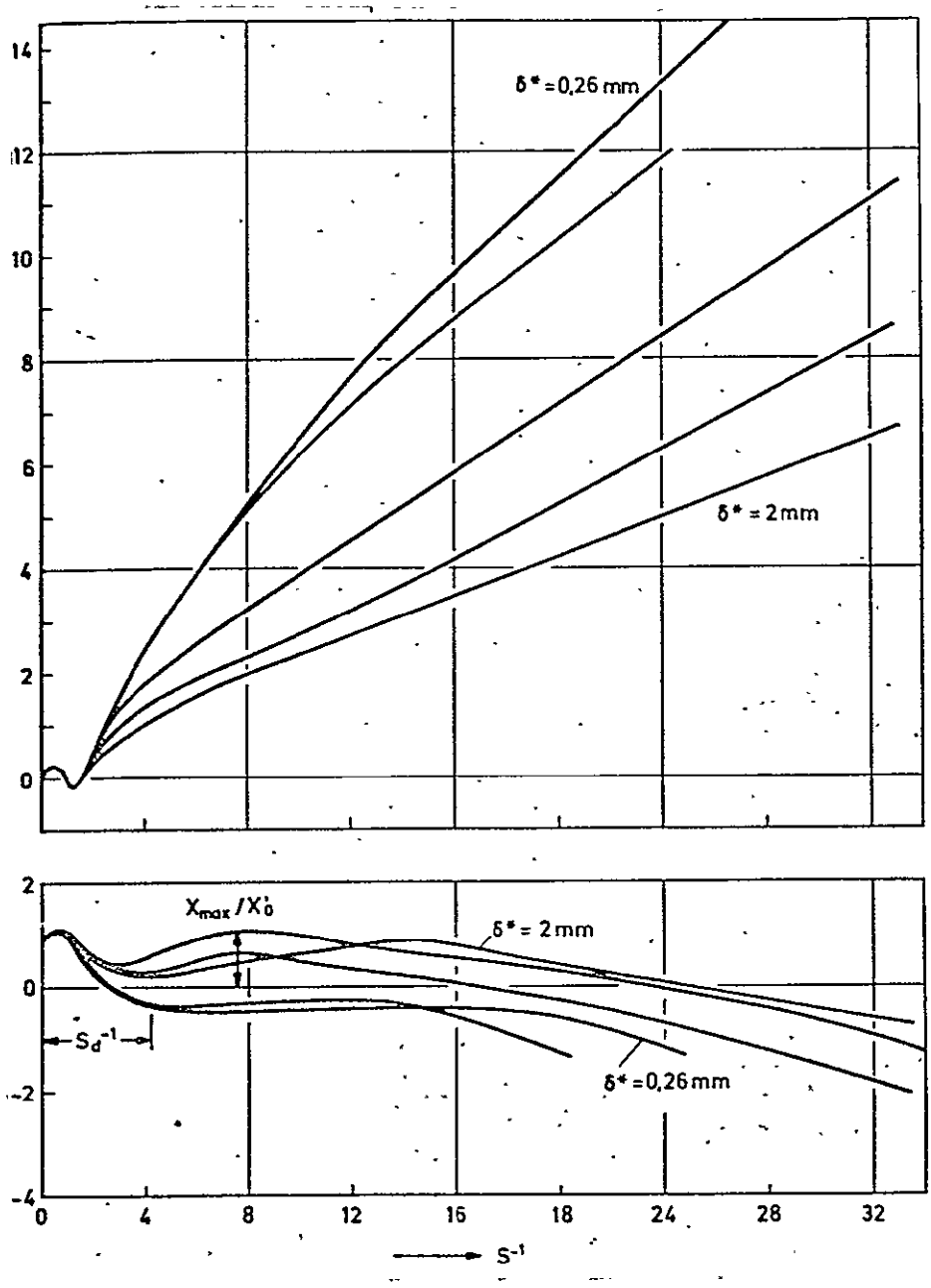

Figure 15: Real and imaginary parts of the impedance of the end correction of an opening (a = 2 mm) for different boundary layer thicknesses. Relationships of Figure 11.

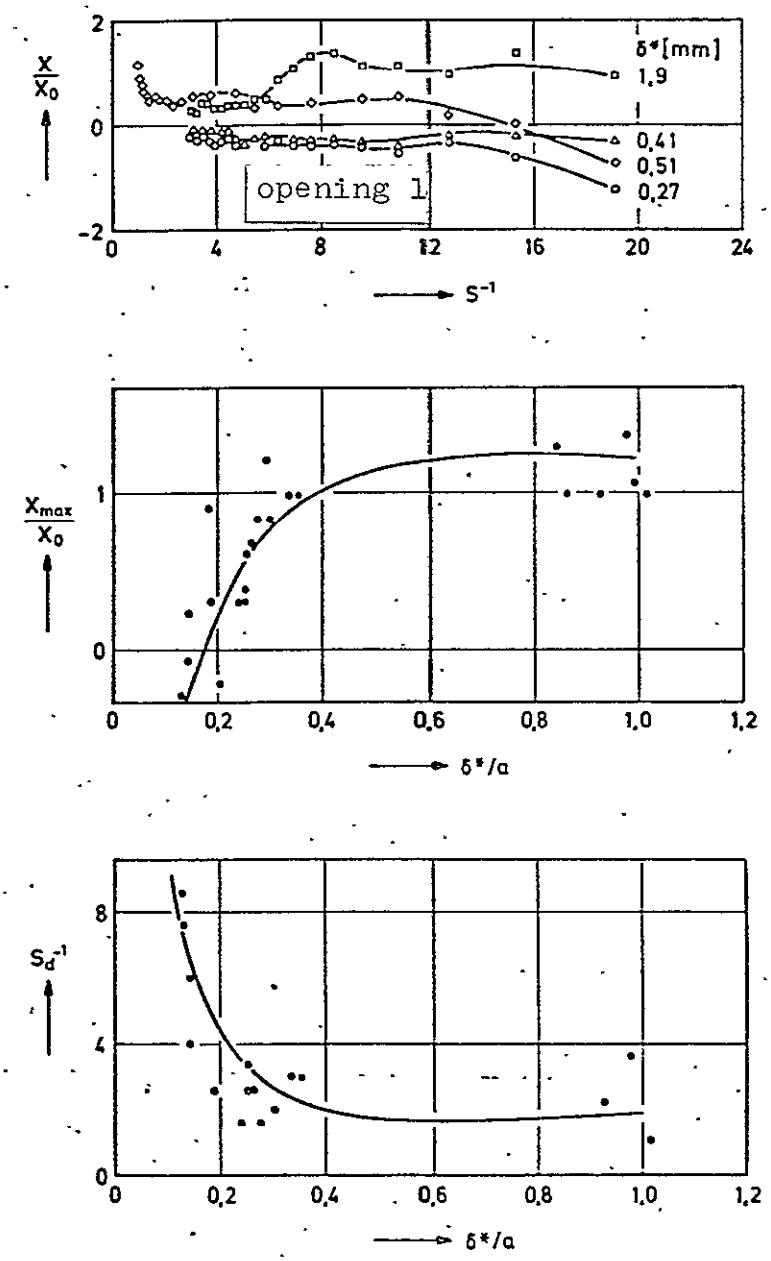

Figure 16: Imaginary part of impedance of the end correction opening (a = 2 mm).

a) for different boundary layer thicknesses U = 40.3 m/s)

b) Second maximum of the imaginary part ,center.

c) Reciprocal Strouhal number, where the curve deviated from the curve for the thinnest boundary layer.

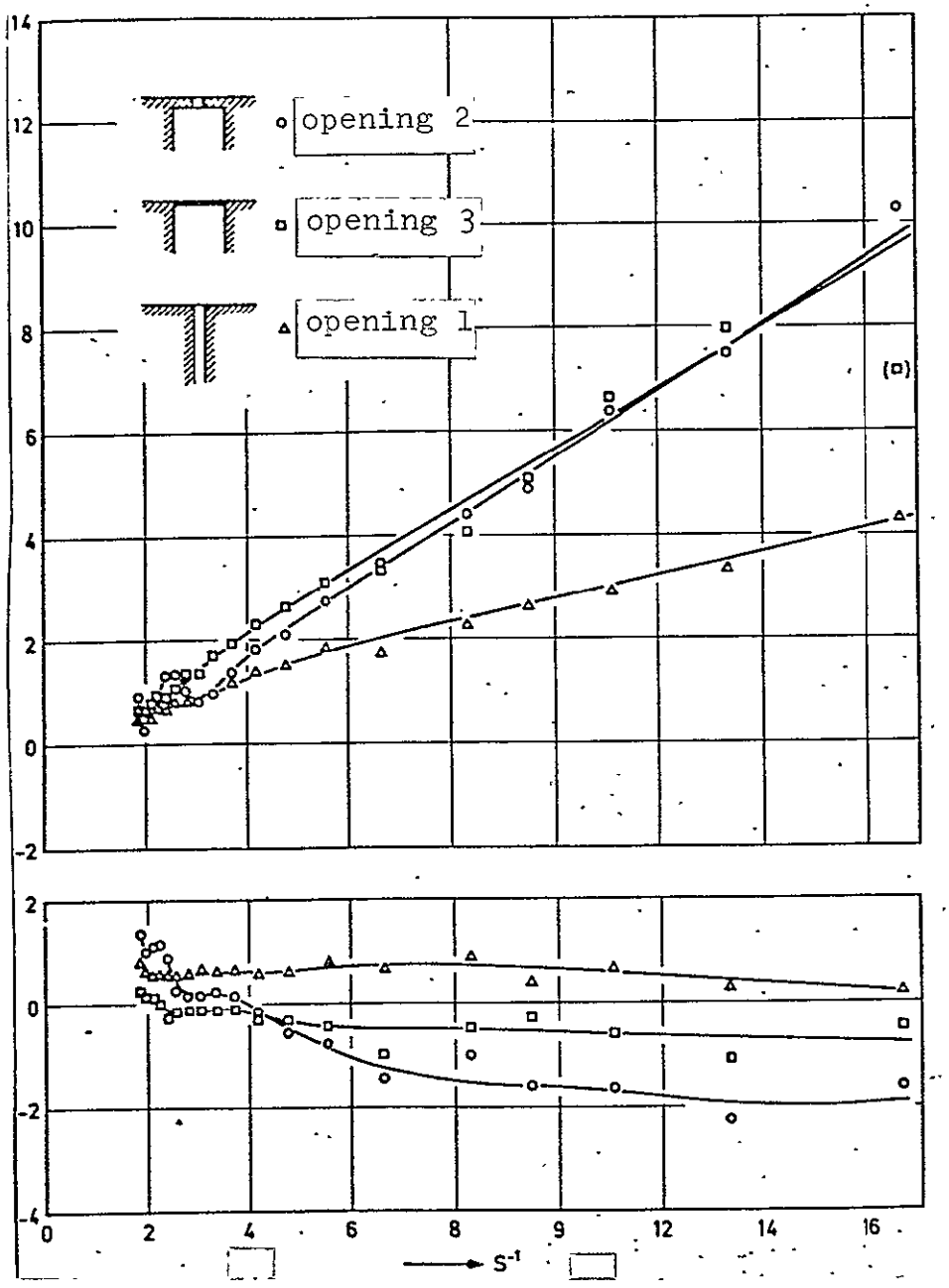

Figure 17: Real and imaginary part of the impedance of the end correction of an opening (a = 2 mm) for different opening lengths (Δ measurement configuration A, o, ▫ measurement configuration B). U = 69.8 m/s, δ^* = 0.68 mm).

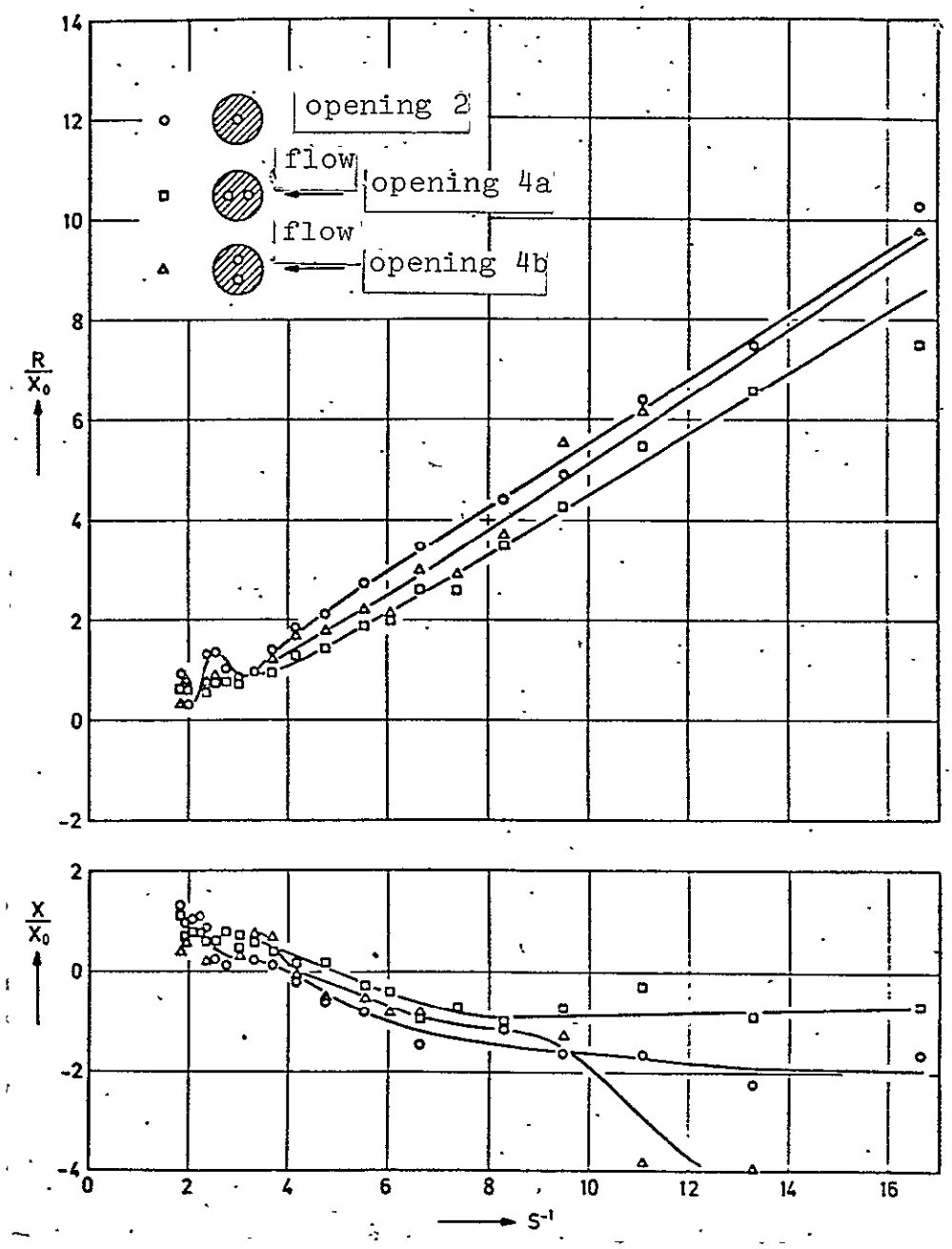

Figure 18: Real and imaginary parts of the impedance of the end correction of an opening (a = 2 mm) for 2 adjacent openings (U = 69.8 m/s, δ^* = 0.68 mm).

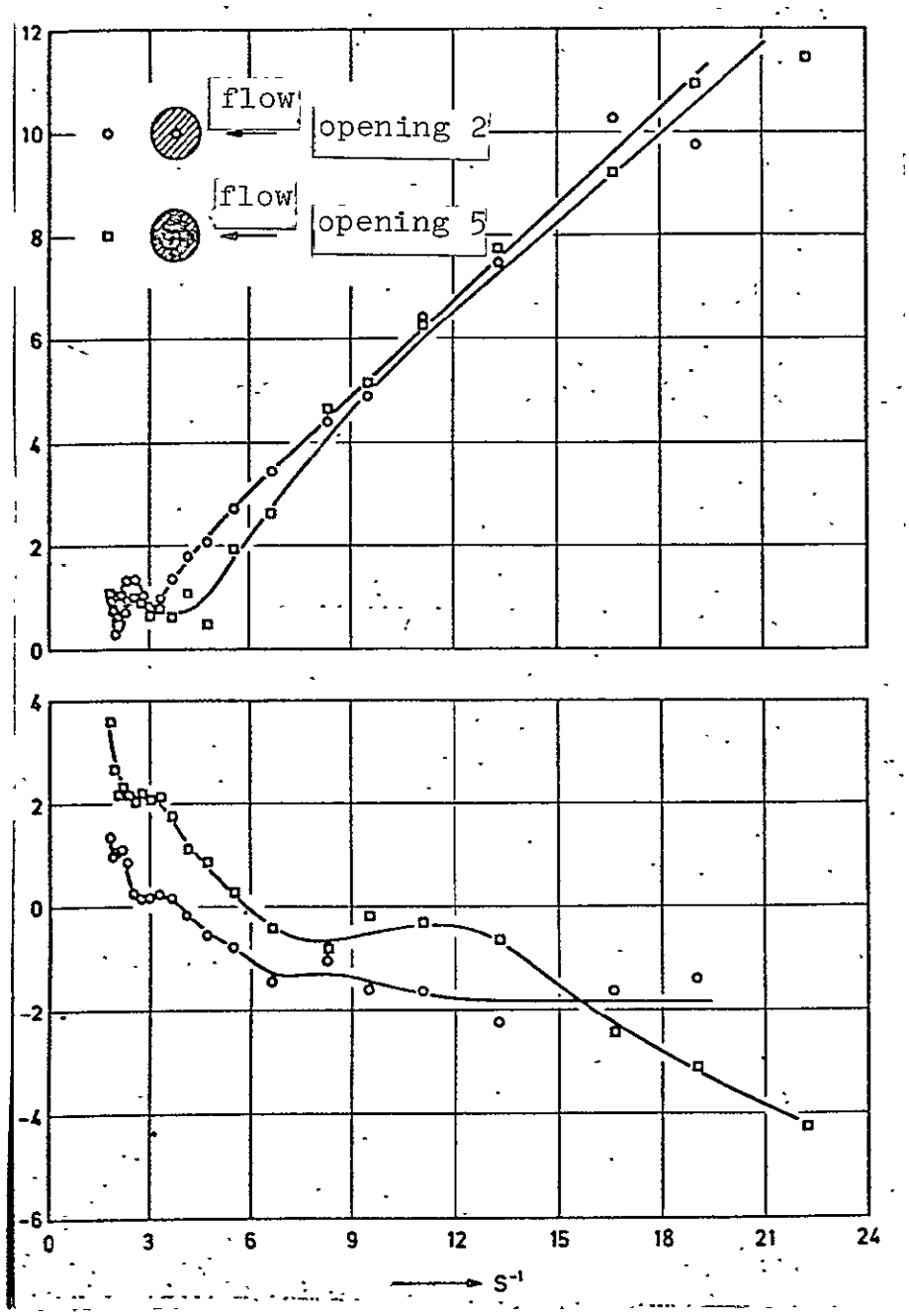

Figure 19: Real and imaginary parts of the impedance of the end correction of an opening (a = 2 mm) for nine adjacent openings (U = 69.8 m/s, δ^* = 0.68 mm).

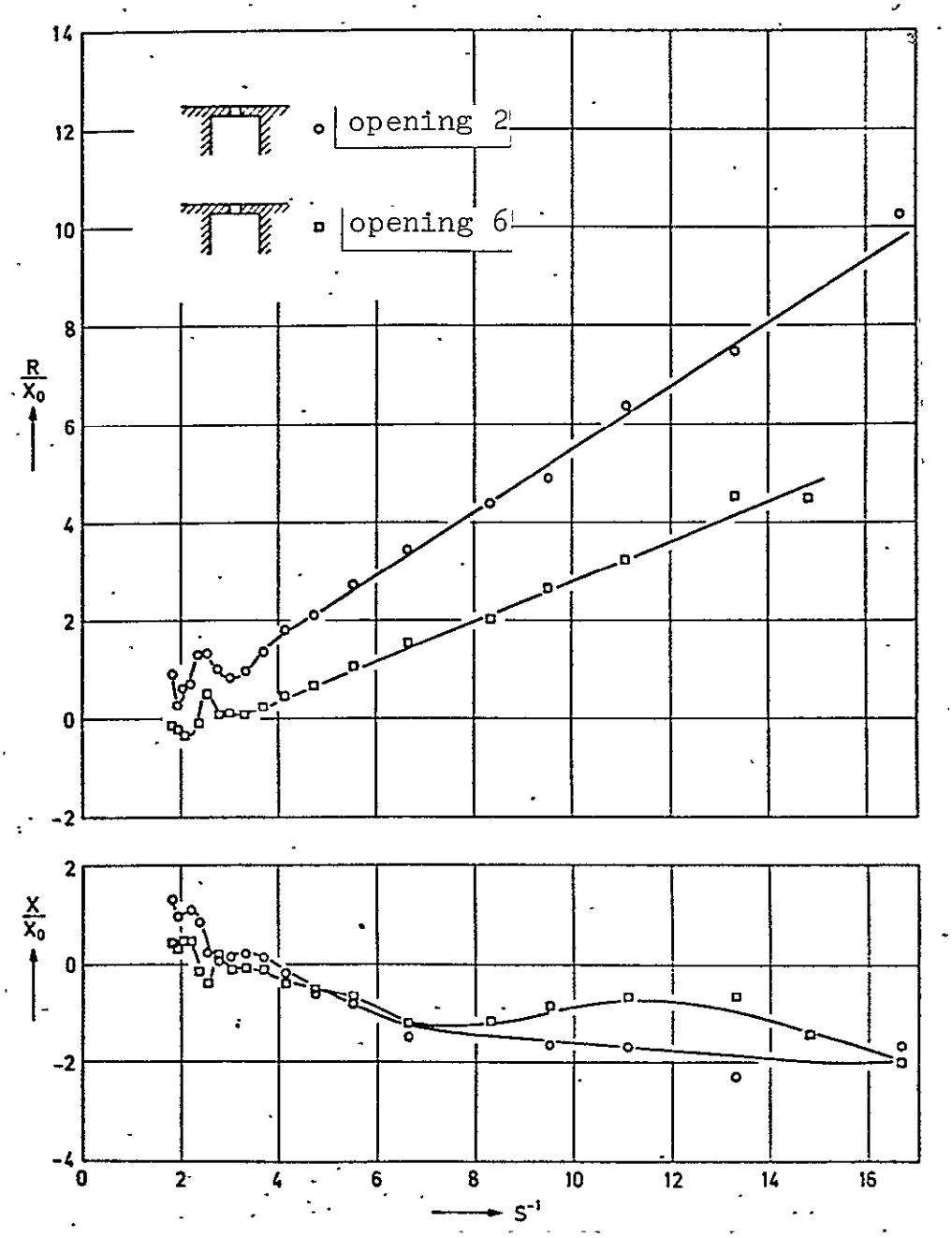

Figure 20: Real and imaginary parts of the impedance of the end correction of an opening (a = 2 mm) with rounded off upper edge (U = 69.8 m/s, δ^* = 0.68 mm).

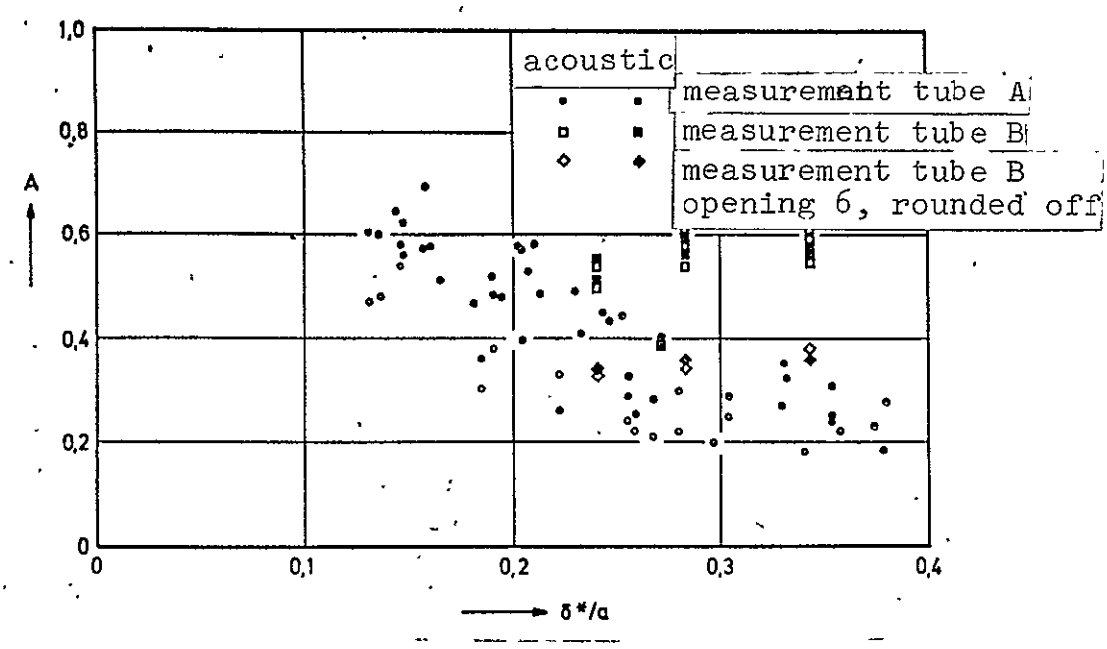

Figure 21: A compared for both measurement configurations.

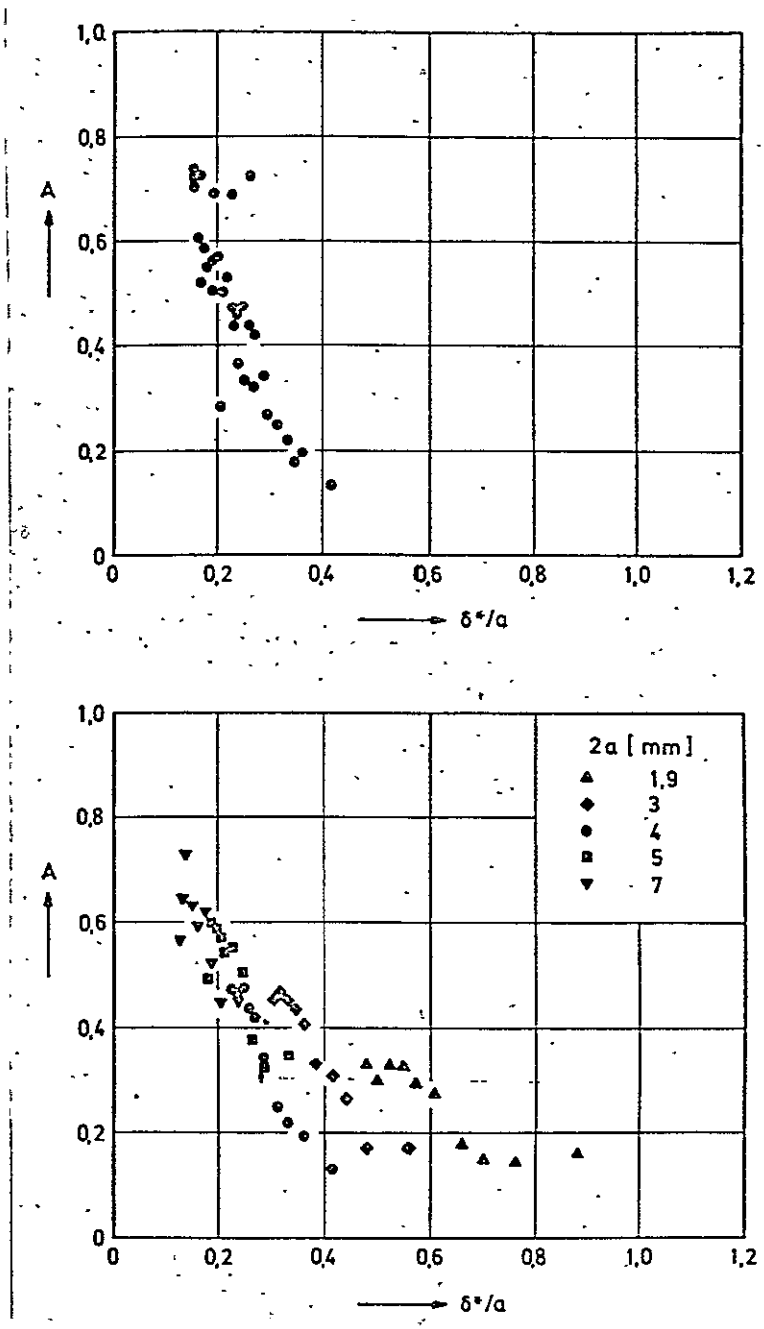

Figure 22: Value of A from uniform flow measurements.

a) For one opening, a = 2 mm, l = 4 mm) for different boundary layer thicknesses (top).

b) for openings of different diameters, the same boundary layer thickness.